Excitonic pairing and insulating transition in two-dimensional semi-Dirac semimetals

Jing-Rong Wang,[1,2] Guo-Zhu Liu,[2,*] and Chang-Jin Zhang[1,3,†]

[1]*High Magnetic Field Laboratory, Hefei Institutes of Physical Science, Chinese Academy of Sciences, Hefei, Anhui 230031, P. R. China*

[2]*Department of Modern Physics, University of Science and Technology of China, Hefei, Anhui 230026, P. R. China*

[3]*Collaborative Innovation Center of Advanced Microstructures, Nanjing University, Nanjing 210093, P. R. China*

arXiv:1611.00145v1 [cond-mat.str-el] 1 Nov 2016

A sufficiently strong long-range Coulomb interaction can induce excitonic pairing in gapless Dirac semimetals, which generates a finite gap and drives semimetal-insulator quantum phase transition. This phenomenon is in close analogy to dynamical chiral symmetry breaking in high energy physics. In most realistic Dirac semimetals, including suspended graphene, Coulomb interaction is too weak to open an excitonic gap. The Coulomb interaction plays a more important role at low energies in a two-dimensional semi-Dirac semimetal than a Dirac semimetal, and indeed leads to breakdown of Fermi liquid theory. We study dynamical excitonic gap generation in a two-dimensional semi-Dirac semimetal by solving the Dyson-Schwinger equation, and show that a moderately strong Coulomb interaction suffices to induce excitonic pairing. Additional short-range four-fermion coupling tends to promote excitonic pairing. Among the available semi-Dirac semimetals, we find that TiO_2/VO_2 nanostructure provides a promising candidate for the realization of excitonic insulator. We also apply the renormalziation group method to analyze the strong coupling between the massless semi-Dirac fermions and the quantum critical fluctuation of excitonic order parameter at the semimetal-insulator quantum critical point, and reveal non-Fermi liquid behaviors of semi-Dirac fermions.

I. INTRODUCTION

The past decade has witnessed the appearance of a huge amount of experimental and theoretical work on the physical properties of various semimetals, in which the valence and conduction bands touch at isolated points [1–3]. The low-energy elementary excitations in these semimetals are various types of massless fermions. The fermion density of state (DOS) vanishes at band-touching points, so the Coulomb interaction remains long-ranged. This is in sharp contrast to the ordinary metals featuring a finite Fermi surface, where Coulomb interaction becomes short-range due to static screening.

Graphene is a two-dimensional (2D) Dirac semimetal with massless Dirac fermions being its low-energy excitations [4, 5]. The surface state of three-dimensional (3D) topological insulator (TI) is also a 2D Dirac semimetal [6, 7]. Apart from these two examples, there are also a number of other systems that support low-energy bulk massless Dirac or Weyl fermions. For instance, a 3D Dirac semimetal emerges at the quantum critical point (QCP) between a trivial band insulator and a topological insulator [8–11]. Moreover, stable 3D Dirac semimetal, protected by crystal symmetry, has been found to exist in Na_3Bi [12] and Cd_3As_2 [13–15]. 3D Weyl semimetal, which hosts fermions with linear dispersion around pairs of Weyl points with opposite chirality, was observed in TaAs [16–19], NbAs [20], TaP [21, 22], and NbP [23, 24] by angle-resolved photoemission spectroscopy (ARPES) experiments. Several other types of semimetals, including 3D quadratic semimetal [25, 26], 3D anisotropic Weyl semimetal [27], 3D double Weyl semimetal [28, 29], 3D nodal-line semimetal [30–33], and 2D semi-Dirac semimetal [34, 35], are also widely investigated.

The effects of long-range Coulomb interaction have been studied in various types of semimetals [5, 34–51]. The role of Coulomb interaction depends crucially on the fermion dispersion and the dimension. Extensive renormalization group (RG) analysis [52] have revealed that Coulomb interaction is marginally irrelevant in 2D Dirac semimetal [5, 36, 37], 3D Dirac/Weyl semimetal [38–41], and also 3D double Weyl semimetal [48, 49]. The Fermi liquid (FL) theory is valid in these systems. However, the Coulomb interaction cannot be simply neglected since it leads to fermion velocity renormalization and logarithmic-like correction to some of the observable quantities [5, 53–58]. Indeed, the predicted velocity renormalization has already been observed in ultra clean suspended graphene [59], quasi-freestanding graphene on silicon carbide (SiC) [60], and graphene on boron nitride substrate [61]. There is also experimental evidence for the renormalization of fermion dispersion in TI-like system of Bi bilayer grown on Bi_2Se_3 [62], which seems to be caused by Coulomb interaction. In a 3D semimetal with quadratic dispersion, the Coulomb interaction is found to be relevant and cause non-Fermi liquid (NFL) behaviors [42]. It is interesting to notice that recent ARPES experiments have discovered NFL behavior in a 3D quadratic semimetal material $Pr_2Ir_2O_7$ [63]. Moreover, in a 3D anisotropic Weyl semimetal [47] and a 3D nodal-line semimetal [50], the FL description is robust because the Coulomb interaction is irrelevant.

In an interacting 2D Dirac fermion system, an intriguing property is that the strong Coulomb interaction might bind a gapless fermion and a gapless hole to form

*Corresponding author: gzliu@ustc.edu.cn

†Corresponding author: zhangcj@hmfl.ac.cn

an excitonic pair, which generates a finite energy gap at the Dirac points and turns the Dirac semimetal into an excitonic insulator [5, 64, 65]. This picture is very similar to the non-perturbative phenomenon of dynamical chiral symmetry breaking (DCSB) that has been extensively investigated in high energy physics [66] since the pioneering work of Nambu and Jona-Lasino [67]. In QCD, the current quarks are massless, but acquire a dynamical mass due to the strong interaction mediated by gluons. The dynamical quark mass breaks the chiral symmetry that is preserved by massless quarks. In a 2D Dirac semimetal, the dynamical fermion mass gap breaks the sublattice symmetry respected by massless Dirac fermions.

According to theoretical analysis [5, 64], an excitonic gap can be dynamically generated in zero external magnetic field only when the effective strength of Coulomb interaction, denoted by the parameter α, is larger than certain critical value. The critical value α_c defines a QCP that separates the semimetallic and excitonic insulating phases. This issue has been most extensively studied in the context of undoped graphene [5, 64, 65]. Physically, the excitonic insulating transition corresponds to the formation of a charge density wave (CDW) order [5, 64]. If the ground state of suspended graphene is an excitonic insulator, there would be more practical applications of graphene in the design of electronic devies [5, 65]. From a theoretic point of view, this provides an ideal laboratory to test some important concepts of high energy physics [68, 69], and also gives us a nice platform to study the rich quantum critical phenomena.

In graphene and other Dirac semimetals, the effective strength of Coulomb interaction can be quantified by the ratio between the Coulombic potential energy and kinetic energy of fermions, defined as [5] $\alpha = e^2/v\epsilon$, where e is the electric charge, v fermion velocity, and ϵ dielectric constant. Experiments have determined that the fermion velocity is $v \approx c/300 \approx 10^5 m/s$, where c is the speed of light in vacuum [4, 5]. For graphene on SiO_2 substrate, $\alpha \approx 0.78$. When graphene is suspended in vacuum, α takes its largest value $\alpha \approx 2.2$ [65], which implies that excitonic pairing is most possibly realized in suspended graphene. To specify whether suspended graphene has a semimetallic or insulating ground state, one needs to calculate the critical value α_c and then compares it with $\alpha \approx 2.2$. The value of α_c has been evaluated by means of several different methods, including Dyson-Schwinger (DS) equation [64, 70–83], Bethe-Salpeter (BS) equation [84–86], RG approach [86–89], and Monte Carlo simulations [90–97]. Drut and Lähde claimed that $\alpha_c \approx 1.1$ in a 2D Dirac fermion system [90, 91], which indicates that graphene placed on SiO_2 substrate is semimetallic but suspended graphene is insulating at zero temperature. Studies based on DS equation [71, 72, 74, 77, 78], BS equation [84, 85], and RG analysis [87–89] all showed that $\alpha_c < 2.2$ and hence also predicted an insulating ground state of suspended graphene. However, experiments clearly revealed that suspended graphene remains a semimetal down to very low temperature, without any sign of insulating behavior [59, 98], which is apparently inconsistent with earlier theoretical results. A number of improved studies [79, 80, 82, 83, 96, 97] have been accomplished to reconcile this discrepancy. After taking into account the influence of fermion velocity renormalization and fermion damping, it was showed in a refined DS equation analysis [79] that the critical value is $\alpha_c \approx 3.3$, which is much larger than $\alpha = 2.2$. Thus it turns out that the Coulomb interaction in suspended graphene is still too weak to open an excitonic gap. Subsequent DS equation computations [80, 82, 83] reached the same qualitative conclusion. By considering the screening of Coulomb interaction due to σ-band electrons [99], recent Monte Carlo simulations also found that α_c is greater than 2.2 [96, 97], which suggests a semimetallic ground state of suspended graphene.

Since graphene cannot be an excitonic insulator, we turn to consider other types of semimetal where the Coulomb interaction plays a more important role. Among the existing semimetal materials, we find that 2D semi-Dirac semimetal provides a better candidate for the realization of excitonic insulating transition than graphene. The dispersion for 2D semi-Dirac fermion is

$$E = \pm\sqrt{ak_x^4 + v^2k_y^2}, \tag{1}$$

which is linear along one momentum component (k_y) but quadratic along the other one (k_x). Such fermions can emerge at the QCP between a 2D Dirac semimetal and a band insulator upon merging two separate Dirac points into a single one. Generation of semi-Dirac fermions through merging of pairs of Dirac point is theoretically predicted to exist in deformed graphene [100–104], pressured organic compound α-(BEDT-TTF)$_2$I$_3$ [102, 104–106], few-layer black phosphorus subject to pressure or perpendicular electric field [107, 108] or doping [109], and some artificial optical lattices [110, 111]. Experimentally, the merging of distinct Dirac points and the appearance of semi-Dirac fermions were recently observed in ultracold Fermi gas of ^{40}K atoms in honeycomb lattice [112], and microwave cavities with graphene-like structure [113]. Kim *et al.* [114] realized semi-Dirac semimetals in few-layer black phosphorus at critical surface doping with potassium. Robust semi-Dirac semimetal state was also predicted to appear in TiO_2/VO_2 nanostructure under suitable conditions [115–117]. It was suggested by first-principle calculations that semi-Dirac fermions may emerge in strained puckered arsenene [118, 119].

The influence of long-range Coulomb interaction in 2D semi-Dirac fermion system was recently investigated by pertubative RG method to one-loop order [34, 35], which showed that Coulomb interaction becomes anisotropic due to dynamical screening [34, 35]. When the bare value of interaction strength α is in the strong coupling regime, the Coulomb interaction induces an anomalous dimension for fermions and produces NFL behaviors over a wide range of intermediate energies [34]. This property is qualitatively similar to graphene [55]. Regardless of the

concrete value of α, the kinetic energy of fermions is enhanced as the renormalized a and v increase with lowering energy. This drives α to flow to zero in the low-energy region very slowly, which means the Coulomb interaction in 2D semi-Dirac semimetal is marginally irrelevant. However, 2D semi-Dirac semimetal differs from graphene in one important aspect. In graphene, the quasiparticle residue Z_f flows to a finite value and thus the system is actually a normal FL despite of the existence of strong velocity renormalization [5, 54, 56]. In contrast, in a 2D semi-Dirac semimetal, Z_f flows to zero in the low-energy regime quite slowly, and the system is a marginal Fermi liquid in the lowest energy limit [34]. This difference indicates that the Coulomb interaction plays a more important role in 2D semi-Dirac semimetal than graphene. It might be possible to form excitonic insulator in some realistic 2D semi-Dirac semimetal.

Dynamical excitonic gap generation is a genuine non-perturbative phenomenon, and cannot be obtained within the framework of ordinary leading-order perturbative calculation [34, 35]. In this paper, we study the possibility of dynamical gap generation in a 2D semi-Dirac semimetal by solving the self-consistent DS integral equation of the excitonic gap. The DS equation is formally very complicated, so it is usually necessary to make some approximations. After solving the DS equation by employing three frequently used approximations, we show that a moderately strong Coulomb interaction suffices to generate an excitonic gap, and that it is easier to realize an excitonic insulating state in a 2D semi-Dirac semimetal than in a 2D Dirac semimetal. Among the currently known semi-Dirac semimetals, we find that the TiO_2/VO_2 nanostructure is a particularly promising candidate to realize excitonic insulating state. One reason is that the such nanostructure is an intrinsic semi-Dirac fermion system, without necessity of fine tuning. The other reason is that the physical value of α in this nanostructure is either smaller or very close to the critical value α_c obtained in our DS equation calculations. Apart from the long-range Coulomb interaction, there may be some additional short-range four-fermion couplings in real materials. Adding such coupling to the system reduces the critical value α_c, and hence catalyzes dynamical excitonic gap generation.

In the insulating phase, the fermions are massive and the systems exhibits different properties than the semimetal phase. We calculate DOS and specific heat of the insulating phase, and compare them with those of semimetal phase. Moreover, we perform a systematic RG analysis of the Yukawa-type coupling between massless fermions and the quantum fluctuation of excitonic order parameter at the QCP of semimetal-insulator transition, and find NFL behaviors of massless fermions. We also study the interplay of this Yukawa coupling with long-range Coulomb interaction. In this case, the massless fermions still exhibit NFL behaviors, but some model parameters behave quite differently from those obtained in the case without Coulomb interaction.

The rest of the paper will be organized as follows. We present the Hamiltonians and the propagators in Sec. II. In Sec. III, we derive the self-consistent gap equation, and numerically solve the gap equation in several different approximations which were employed in the studies of the excitonic gap equation in graphene. We compare our results for semi-Dirac semimetal and previous results for graphene carefully in this section. In Sec. IV, we study the dynamical gap generation including long-range Coulomb interaction and additional four-fermion interaction. The impact of excitonic gap for several observable quantities and the NFL behaviors of the fermions at the QCP between semi-Dirac semimetal phase and excitonic insulating phase are shown in Sec. V. We summarize the main results in Sec. VI.

II. MODEL HAMILTONIAN

The Hamiltonian for free 2D semi-Dirac fermions is

$$H_{\rm f}=\sum_{\sigma=1}^{N}\int d^2x\psi_\sigma^\dagger(\mathbf{x})\left[-a\nabla_x^2\tau_1-iv\nabla_y\tau_2\right]\psi_\sigma(\mathbf{x}), \quad (2)$$

where ψ_σ represents the two-component spinor field with flavor index $\sigma=1,2,3,...,N$, and $\tau_{1,2,3}$ are standard Pauli matrices. The spinor ψ_σ can be written as $\psi_\sigma=(\psi_{A\sigma},\psi_{B\sigma})^T$, where A and B are two sublattice indices [101, 103, 120]. Two model parameters a and v are introduced to characterize the fermion energy spectrum. The fermions are subject to a long-range Coulomb interaction, given by

$$H_{\rm C}=\frac{1}{4\pi}\sum_{\sigma=1}^{N}\int d^2xd^2x'\rho_\sigma(\mathbf{x})\frac{e^2}{\epsilon\left|\mathbf{x}-\mathbf{x}'\right|}\rho_\sigma^\dagger(\mathbf{x}'), \quad (3)$$

where the fermion density operator is defined as

$$\rho_\sigma(\mathbf{x})=\psi_\sigma^\dagger(\mathbf{x})\psi_\sigma(\mathbf{x}).$$

The model will be treated by making perturbative expansion in powers of $1/N$.

The free fermion propagator reads

$$G_0(\omega,\mathbf{k})=\frac{1}{-i\omega+ak_x^2\tau_1+vk_y\tau_2}. \quad (4)$$

The bare Coulomb interaction is written in the momentum space as

$$V_0(\mathbf{q})=\frac{2\pi e^2}{\epsilon|\mathbf{q}|}=\frac{2\pi\alpha v}{|\mathbf{q}|}, \quad (5)$$

where $\alpha=e^2/\epsilon v$ represents the effective interaction strength. After including the dynamical screening, the dressed Coulomb interaction function can be written as

$$V(\Omega,\mathbf{q})=\frac{1}{V_0^{-1}(\mathbf{q})+\Pi(\Omega,\mathbf{q})}, \quad (6)$$

in which the polarization function $\Pi(\Omega, \mathbf{q})$ is given by

$$\Pi(\Omega, \mathbf{q}) = -N \int \frac{d\omega}{2\pi} \mathrm{Tr}\left[G_0(\omega, \mathbf{k}) G_0(\omega + \Omega, \mathbf{k} + \mathbf{q})\right] \quad (7)$$

to the leading order of $1/N$ expansion. It is technically quite difficult to obtain a complete analytical expression of $\Pi(\Omega, \mathbf{q})$. The recent work of Isobe *et al.* [34] found that $\Pi(\Omega, \mathbf{q})$ can be approximated by the expression

$$\begin{aligned} \tilde{\Pi}(\Omega, q_x, q_y) &= \frac{N}{v} \frac{d_x a^{1/2} q_x^2}{\left(\Omega^2 + c_0 a^2 q_x^4 + v^2 q_y^2\right)^{1/4}} \\ &+ \frac{N}{v} \frac{d_y a^{-1/2} v^2 q_y^2}{\left(\Omega^2 + c_0 a^2 q_x^4 + v^2 q_y^2\right)^{3/4}}, \end{aligned} \quad (8)$$

which produces the precise analytical expressions of $\Pi(\Omega, \mathbf{q})$ in several different limits. In this expression, d_x, d_y, and c_0 are three constants:

$$\begin{aligned} d_x &= \frac{1}{8\sqrt{\pi}} \frac{\Gamma(3/4)}{\Gamma(9/4)}, \quad d_y = \frac{1}{8\sqrt{\pi}} \frac{\Gamma(5/4)}{\Gamma(7/4)}, \\ c_0 &= \left(\frac{2}{\sqrt{\pi}} \frac{\Gamma(3/4)}{\Gamma(9/4)}\right)^4. \end{aligned} \quad (9)$$

If the fermions dynamically acquire a finite mass m due to Coulomb interaction, a new term will be added to the total Hamiltonian

$$\begin{aligned} H_m &= m \sum_{\sigma=1}^{N} \int \frac{d^2\mathbf{k}}{(2\pi)^2} \psi_\sigma^\dagger \tau_3 \psi_\sigma \\ &= m \sum_{\sigma=1}^{N} \int \frac{d^2\mathbf{k}}{(2\pi)^2} \left(\psi_{A\sigma}^\dagger \psi_{A\sigma} - \psi_{B\sigma}^\dagger \psi_{B\sigma}\right). \end{aligned} \quad (10)$$

It is easy to observe that the dynamically generated mass m breaks the exchanging symmetry between sublattices A and B. Therefore, the excitonic gap leads to the formation of CDW state.

III. DYSON-SCHWINGER EQUATION OF EXCITNONIC GAP

Since excitonic gap generation is a non-perturbative phenomenon, it cannot be investigated by making ordinary perturbative calculations. This issue will be studied by analyzing the DS equation, which is non-perturbative in nature and provides an ideal tool of describing various phase transitions. Since Nambu and Jona-Lasinio [67], the DS equation approach has been widely applied to study DCSB in QCD [121, 122] and QED$_3$ [123–128]. It also has been used to examine whether an excitonic gap can be dynamically generated by the Coulomb interaction in graphene [64, 68, 70–83] and other closely related materials [41, 46, 82]. The role played by DS equation in studying excitonic gap generation is the same as the gap equation in studying the formation of superconductivity in BCS theory. In this section, we will compute the critical interaction strength α_c for excitonic insulating transition by solving the DS equation of fermion gap.

The full fermion propagator can be written as

$$G_F(\omega, \mathbf{k}) = \frac{1}{-A_0 i\omega + A_1 a k_x^2 \tau_1 + A_2 v k_y \tau_2 + m\tau_3}. \quad (11)$$

Here, we introduce $A_{0,1,2} \equiv A_{0,1,2}(\omega, k_x, k_y)$ to represent the renormalized functions, and use $m \equiv m(\omega, k_x, k_y)$ to represent the dynamically generated fermion mass. The full and free fermion propagators are connected by the following DS equation

$$G_F^{-1}(\varepsilon, \mathbf{p}) = G_0^{-1}(\varepsilon, \mathbf{p}) + \Sigma(\varepsilon, \mathbf{p}), \quad (12)$$

where the fermion self-energy function is

$$\Sigma(\varepsilon, \mathbf{p}) = \int \frac{d\omega}{2\pi} \frac{d^2\mathbf{k}}{(2\pi)^2} G_F(\omega, \mathbf{k}) \Gamma_{\varepsilon, \mathbf{p}, \omega, \mathbf{k}} V(\Omega, \mathbf{q}) \quad (13)$$

with $\Omega = \varepsilon - \omega$ and $\mathbf{q} = \mathbf{p} - \mathbf{k}$. The function $\Gamma_{\varepsilon, \mathbf{p}, \omega, \mathbf{k}} \equiv \Gamma(\varepsilon, \mathbf{p}; \omega, \mathbf{k})$ is the vertex correction. In order to make the above equation tractable, it is necessary to truncate the closed equation in a proper way. For simplicity, we assume that $A_0 \equiv 1$, which is justified at large N because the equation of A_0 contains a factor of $1/N$. We also assume $\Gamma \equiv 1$, which naturally satisfies the Ward identity. To further simplify the problem, we take $A_1 = A_2 \equiv 1$.

After making these approximations, we obtain the following non-linear integral equation of fermion mass

$$\begin{aligned} m(\varepsilon, p_x, p_y) &= \int \frac{d\omega}{2\pi} \int \frac{d^2\mathbf{k}}{(2\pi)^2} m(\omega, k_x, k_y) \\ &\times \frac{1}{\omega^2 + a^2 k_x^4 + v^2 k_y^2 + m^2(\omega, k_x, k_y)} \\ &\times V(\varepsilon - \omega, \mathbf{p} - \mathbf{k}). \end{aligned} \quad (14)$$

The solution of this equation is determined by three parameters: Coulomb interaction strength α, fermion flavor N, and a tuning parameter $\beta = a\Lambda/v$, where Λ is a UV cutoff.

The above equation can be numerically solved by the iterative method. Due to the explicit breaking of Lorentz invariance by the static Coulomb interaction and the anisotropic fermion dispersion, the fermion mass gap $m(\varepsilon, p_x, p_y)$ depends on its three free variables separately. Therefore, the above gap equation is formally much more complicated than that in graphene, where the gap equation contains only two independent variables, namely ε and $|p|$. To make sure that our numerical iterations are under control, it is necessary to introduce further approximations to the above gap equation. In the DS equation studies of excitonic gap generation in graphene, there are three frequently used approximations: instantaneous approximation [64, 70–72], Khveshchenko approximation [73], and Gamayun-Gorbar-Gusynin (GGG) approximation [74]. We shall numerically solve the DS equation (14) under these three approximations separately, and then compare the results to those obtained in the context of graphene [64, 70, 71, 73, 74].

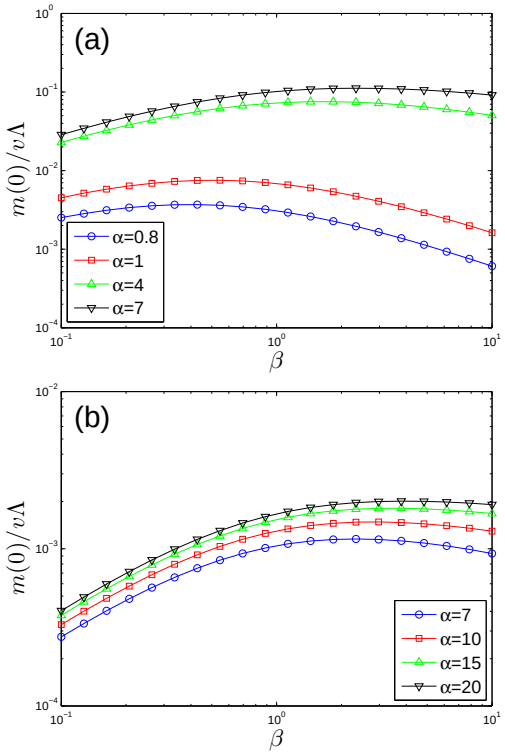

FIG. 1: Dependence of fermion mass $m(0)$ on β obtained under instantaneous approximation at different values of α. (a) $N = 2$; (b) $N = 4$.

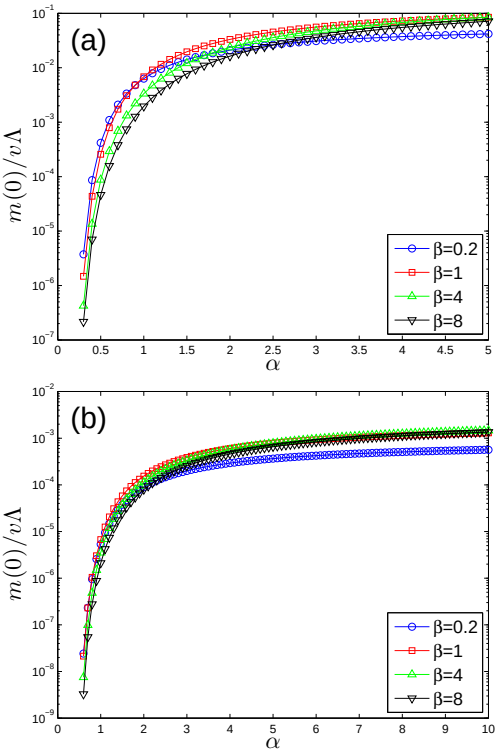

FIG. 2: Dependence of fermion mass $m(0)$ on α obtained under instantaneous approximation at different values of β. (a) $N = 2$; (b) $N = 4$.

A. Instantaneous approximation

The instantaneous approximation is widely employed to simplify the self-consistent DS equation of dynamical fermion gap. It has been used in such 2D Dirac semimetal as graphene [64, 68, 70, 71, 76, 77, 81], 3D semimetal with quadratic touching points [46], and finite temperature QED$_3$ [128]. A universal feature shared by these systems is that the fermion mass gap depends on energy and momentum separately due to the explicit breaking of Lorentz invariance, which makes it very difficult to solve the self-consistent gap equation numerically. In the instantaneous approximation, the energy-dependence of fermion gap is dropped, but the momentum-dependence is maintained. Under this approximation, the interaction function becomes

$$\begin{aligned} V(\Omega,\mathbf{q}) \;\to\; V(\mathbf{q}) &= \frac{1}{V_0^{-1}(\mathbf{q})+\Pi(\mathbf{q})} \\ &= \left[\frac{|\mathbf{q}|}{2\pi\alpha v}+\frac{N}{v}\frac{d_x a^{1/2}q_x^2}{\left(c_0a^2q_x^4+v^2q_y^2\right)^{1/4}}\right. \\ &\quad \left.+\frac{N}{v}\frac{d_y a^{-1/2}v^2q_y^2}{\left(c_0a^2q_x^4+v^2q_y^2\right)^{3/4}}\right]^{-1}. \end{aligned} \tag{15}$$

Accordingly, the gap equation (14) is simplified to

$$\begin{aligned} m(p_x,p_y) \;=\; &\frac{1}{2}\int\frac{d^2\mathbf{k}}{(2\pi)^2}\frac{m(k_x,k_y)}{\sqrt{a^2k_x^4+v^2k_y^2+m^2(k_x,k_y)}} \\ &\times V(\mathbf{p}-\mathbf{k}). \end{aligned} \tag{16}$$

We show the dependence of $m(0)\equiv m(p_x=0,p_y=0)$ on β obtained for $N = 2$ and $N = 4$ in Fig. 1(a) and Fig. 1(b), respectively. It is apparent that $m(0)$ exhibits a non-monotonic dependence on β. As β grows, $m(0)$ increases initially, but begins to decrease once β is greater than some critical value. The dependence of $m(0)$ on parameter α in the cases of $N = 2$ and $N = 4$ is presented in Fig. 2. We can clearly observe that $m(0)$ decreases as α is lowered, and eventually vanishes once α is smaller than a critical value α_c. According to the results given in Fig. 2, it turns out that the critical value α_c is not very sensitive to the change in β. For a series of different values of β, ranging from 0.2 to 8, $\alpha_c \approx 0.6$ in the case of $N = 4$. In a 2D Dirac semimetal, the critical interaction strength obtained under instantaneous approximation is $\alpha_c \approx 2.33$ for $N = 4$ [64, 70]. An immediate indication is that the excitonic gap can be much more easily generated in a 2D semi-Dirac semimetal than a 2D Dirac semimetal.

For fixed values of α and β, there exists a critical fermion flavor N_c that separates the semimetallic and excitonic insulating phases. As shown in Fig. 3, $m(0)$

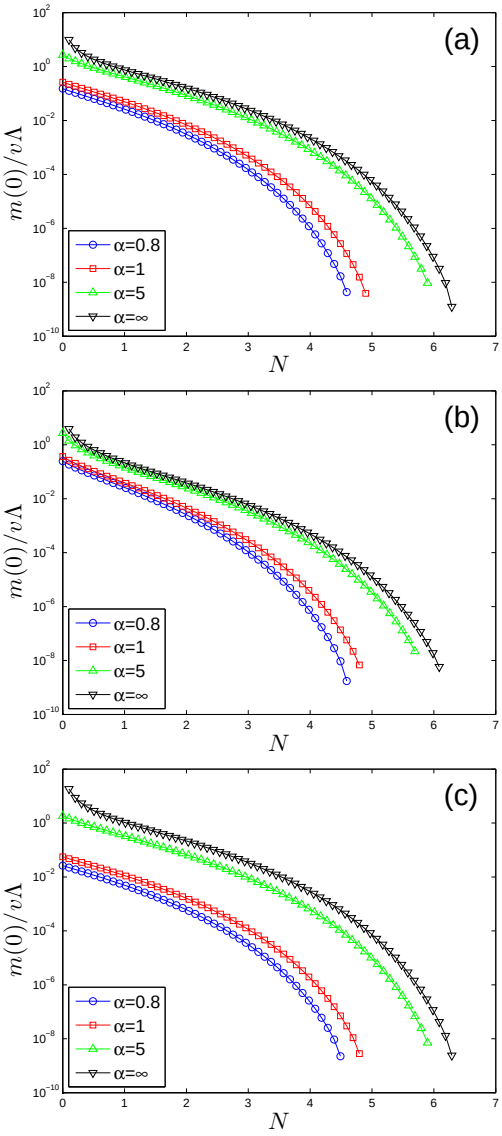

FIG. 3: Dependence of fermion mass $m(0)$ on N obtained under instantaneous approximation at different values of α. (a) $\beta = 1$, (c) $\beta = 0.1$, and (c) $\beta = 10$.

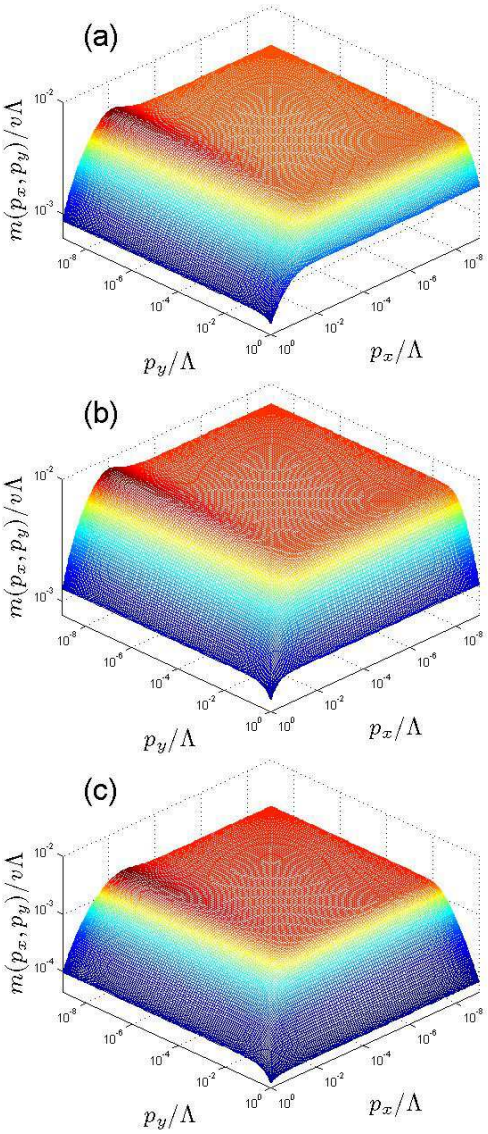

FIG. 4: Dependence of $m(p_x, p_y)$ on p_x and p_y obtained under instantaneous approximation at $\alpha = 1$ and $N = 2$. (a) $\beta = 0.1$; (b) $\beta = 1$; (c) $\beta = 10$.

decreases with growing N and vanishes once N exceeds N_c. Specifically, N_c takes a finite value even in the infinitely strong coupling limit $\alpha \to \infty$. Thus, the flavor N must be sufficiently small for an excitonic gap to be opened. Moreover, Fig. 3 tells us that, N_c always falls in the range of $(6, 7)$ in the $\alpha \to \infty$ limit, which is valid for three representative values of β. As a comparison, we recall that $N_c = 8/\pi \approx 2.55$ in the limit $\alpha \to \infty$ in a 2D Dirac semimetal, which was obtained under the same approximation [64, 70]. This result provides further evidence that it is much easier to induce an excitonic gap in a 2D semi-Dirac semimetal than a 2D Dirac semimetal.

To acquire a more quantitative knowledge of the fermion gap, we present function $m(p_x, p_y)$ in Fig. 4. In the limit $p_{x,y} \to 0$, $m(p_x, p_y)$ approaches a finite value $m(0, 0)$. As p_x or p_y grows, $m(p_x, p_y)$ drops rapidly when ap_x^2 or vp_y is larger than the energy scale given by $m(0, 0)$. It appears that $m(p_x, p_y)$ exhibits a weak non-monotonic dependence on p_x in the intermediate range of energies, but $m(p_x, p_y)$ decreases monotonously with growing p_y. The strongly anisotropic behavior of $m(p_x, p_y)$ clearly comes from the anisotropy in fermion dispersion.

B. Khveshchenko approximation

Under the instantaneous approximation, the energy-dependence of Coulomb interaction is entirely ignored. In a 2D Dirac semimetal, after including the one-loop polarization, the dressed Coulomb interaction function is

given by

$$V_{\rm Dirac} = \frac{1}{\frac{|\mathbf{q}|}{2\pi\alpha v} + \frac{N|\mathbf{q}|^2}{16\sqrt{\Omega^2+|\mathbf{q}|^2}}}. \tag{17}$$

Khveshchenko [73] proposed an improved approximation

$$V_{\rm Dirac} \to \frac{1}{\frac{|\mathbf{q}|}{2\pi\alpha v} + \frac{N|\mathbf{q}|}{16\sqrt{2}}}, \tag{18}$$

and then applied it to study dynamical gap generation in graphene [73]. It was shown by Khveshchenko [73] that $\alpha_c \approx 1.13$ for $N = 4$, which is much smaller than $\alpha_c \approx 2.33$ obtained by using the instantaneous approximation. It was also found [73] that $N_c \approx 7.18$ in the strong coupling limit $\alpha \to \infty$, which is much larger than $N_c \approx 2.55$ obtained under instantaneous approximation. It is therefore clear that the energy dependence of Coulomb interaction plays an important role and needs to be seriously incorporated in the DS equation.

We now adopt the Khveshchenko approximation to study the DS gap equation in 2D semi-Dirac semimetal. The dressed Coulomb interaction function given by Eq. (6) can be approximated as

$$V(\mathbf{q}) \to \left[\frac{|\mathbf{q}|}{2\pi\alpha v} + \frac{N}{v}\frac{d_x a^{1/2} q_x^2}{\left(2\left(c_0 a^2 q_x^4 + v^2 q_y^2\right)\right)^{1/4}} + \frac{N}{v}\frac{d_y a^{-1/2} v^2 q_y^2}{\left(2\left(c_0 a^2 q_x^4 + v^2 q_y^2\right)\right)^{3/4}}\right]^{-1}. \tag{19}$$

Under the Khveshchenko approximation, the DS gap equation has the same form as Eq. (16) with $V(\mathbf{p}-\mathbf{k})$ being given by Eq. (19). We then solve this DS equation numerically. At $N = 4$, the dependence of $m(0,0)$ on α is shown in Fig. 5 for several values of β in (a), (b), and (c) respectively, represented by the red line with square mark. We can see that $m(0,0)$ obtained by using Eq. (19) is larger than that obtained by using the instantaneous approximation, which shows that including the energy dependence of Coulomb interaction tends to favor the generation of excitonic gap in 2D semi-Dirac semimetal. Another indication of Fig. 5 is that the critical value α_c does not visibly change within a wide range of values of β. For $\beta = 1, 0.1, 10$, we find $\alpha_c \approx 0.4$, which is much smaller than $\alpha_c \approx 1.13$ obtained in 2D Dirac semimetal under the same approximation [73]. We thus see once again that it is easier for Coulomb interaction to open an excitonic gap in a 2D semi-Dirac semimetal. The relation between $m(0)$ and N is presented in Fig. 6(a) and (b) with $\alpha = 0.1$ and $\alpha = \infty$ respectively. By using the Khveshchenko approximation, it is found that $m(0)$ vanishes once N is greater than some critical value, even in the strong coupling limit $\alpha \to \infty$.

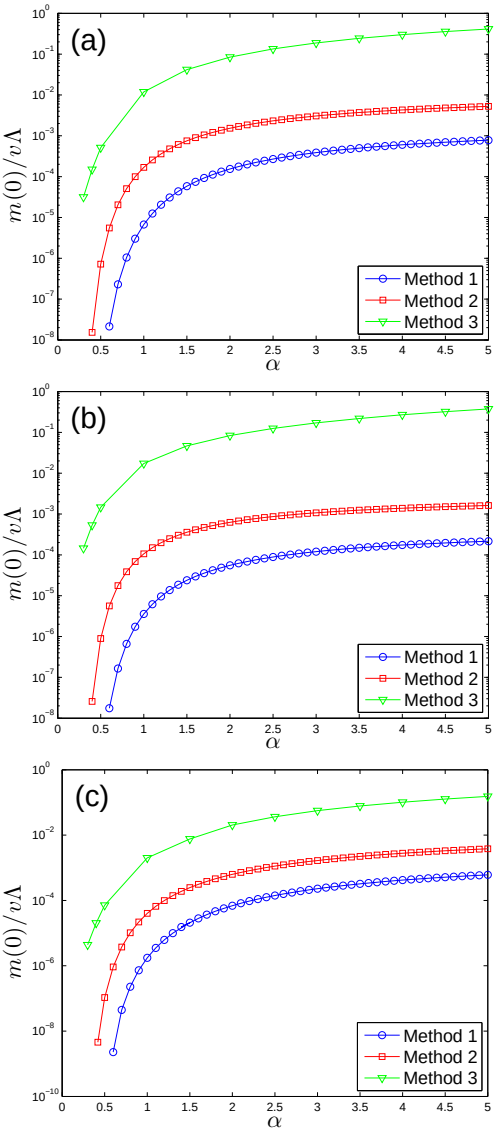

FIG. 5: Dependence of $m(0)$ on α with $\beta = 1$ in (a), $\beta = 0.1$ in (b), and $\beta = 10$ in (c). Method 1: Instantaneous approximation; Method 2: Khveshchenko approximation; Method 3: GGG approximation. This convention is also used in Fig. 6.

C. Gamayun-Gorbar-Gusynin approximation

In order to include the influence of energy dependence of Coulomb interaction on dynamical gap generation in 2D Dirac semimetal, Gamayun *et al.* [74] introduced another approximation, which assumes the mass gap to be energy independent, namely

$$m(\varepsilon, \mathbf{p}) \to m(\mathbf{p}), \tag{20}$$

but retains the energy dependence of Coulomb interaction. Under the GGG approximation, they solved the DS equation and found that $\alpha_c \approx 0.92$ for flavor $N = 4$, which is clearly smaller than $\alpha_c \approx 2.33$ obtained under the instantaneous approximation [64, 70]. This result

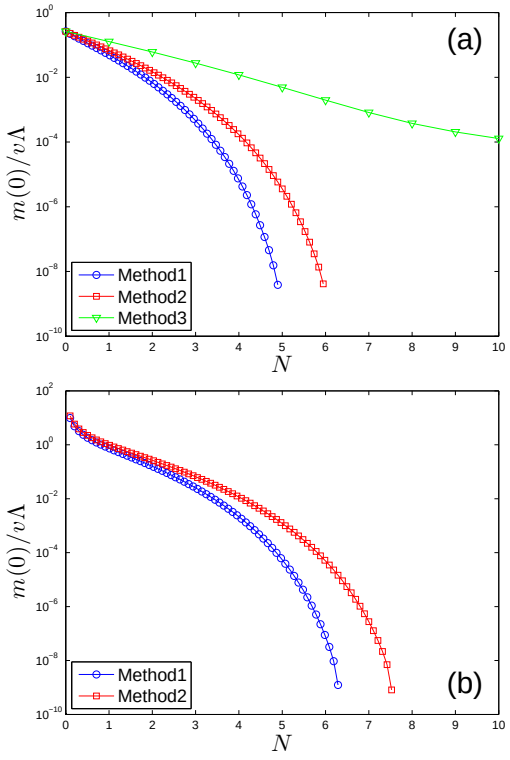

FIG. 6: Dependence of $m(0)$ as a function of flavor N. (a) $\alpha = 1$; (b) $\alpha = \infty$.

provides another signature that the energy dependence of Coulomb interaction is in favor of dynamical excitonic gap generation. They also found that, in the strong coupling limit $\alpha \to \infty$, the critical fermion flavor $N_c \to \infty$, which is quite different from the results obtained under the instantaneous and Khveshchenko approximations.

In this subsection, we employ the GGG approximation to study the dynamical excitonic gap in 2D semi-Dirac semimetal. By applying this approximation, the DS gap equation (14) becomes

$$m(p_x, p_y) = \int \frac{d\omega}{2\pi} \frac{d^2\mathbf{k}}{(2\pi)^2} m(k_x, k_y) \times \frac{1}{\omega^2 + a^2 k_x^4 + v^2 k_y^2 + m^2(k_x, k_y)} \times V(\omega, \mathbf{p} - \mathbf{k}). \quad (21)$$

The relation between $m(0)$ and α with $N = 4$ is shown in Fig. 5 by the green line with the triangular mark. In Fig. 5(a), (b), and (c), β equal to 1, 0.1, and 10 respectively. As shown in Fig. (5), $m(0)$ calculated through Eq. (21) is clearly larger than the one obtained under instantaneous and Khveshchenko approximations, which indicates that energy dependence of Coulomb interaction enhances dynamical gap generation. For $\beta = 1, 0.1, 10$, we find that $\alpha_c < 0.3$, which is also much smaller than $\alpha_c \approx 0.92$ obtained in a 2D Dirac semimetal [74]. It is also clear that an excitonic gap can be more easily opened by Coulomb interaction in a 2D semi-Dirac semimetal.

The dependence of fermion gap on N obtained at $\alpha = 1$ is shown in Fig. 6(a), represented by the green line with triangular mark. The critical flavor N_c is much larger than that obtained under instantaneous and Khveshchenko approximations. In the infinitely strong coupling limit $\alpha \to \infty$, we find that N_c goes to infinity. This stems from an infrared divergence that is owing to the singular contribution appearing in the regions of $aq_x^2 \ll \Omega$ and $vq_y \ll \Omega$. These results point towards the fact that the energy dependence of Coulomb interaction is in favor of dynamical gap generation.

A short summary is necessary here. We have numerically solved the DS equation on the basis of three widely used approximations. Although the critical value of α_c depends on the concrete approximation adopted to solve the equation, we can infer from the extensive numerical solutions that α_c obtained in a 2D semi-Dirac semimetal is much smaller than the one in a 2D Dirac semimetal. It is safe to conclude that a moderately strong Coulomb interaction suffices to open a finite excitonic gap in a 2D semi-Dirac semimetal.

As mentioned in Sec. I, there are indeed several possible ways to obtain a realistic 2D semi-Dirac semimetal. For instance, it can be created by merging two Dirac fermions at the QCP between a 2D Dirac semimetal and a trivial band insulator. Massless 2D semi-Dirac fermions also naturally emerge in a black phosphorus placed in a perpendicular electric field. However, in these cases the semi-Dirac semimetal is realized either by making a delicate tuning of some special parameter or by introducing an external field. It is therefore technically difficult to prepare a robust and intrinsic semi-Dirac semimetal in these materials. In contrast, an intrinsic 2D semi-Dirac semimetal can be more readily achieved in a TiO_2/VO_2 nanostructure, which was proposed by Pardo and his collaborators [115–117].

We now estimate the actual value of the interaction parameter α. In VO_2, the fermion velocity is roughly $v_F \approx 1.5 \times 10^5$m/s [115], and the fermion flavor is $N = 4$ [117]. The value of α relies crucially on the dielectric constant ϵ. In VO_2, the constant $\epsilon \approx 36$ at room temperature, and increases with growing temperature [129]. It was predicted [115] that $\alpha \approx 0.41$ in VO_2 at room temperature. At lower temperatures, the value of ϵ can be made even smaller than 36, which then gives rise to a value of α that is larger than $\alpha \approx 0.41$. The value of ϵ can also be further tuned by other non-thermal scenarios, such as substrate. Our DS equation calculations have showed that the critical parameter $\alpha_c \approx 0.6$, $\alpha_c \approx 0.4$, and $\alpha_c < 0.3$ under the instantaneous, Khveshchenko, and GGG approximations, respectively. We can see that the actual value of α at room temperature is already smaller or close to the critical value α_c. At nearly zero temperatures, the physical value of α might become much larger than 0.41. We thus predict that the TiO_2/VO_2 nanostructure is an ideal candidate to realize excitonic insulator, which can be probed by ARPES [130] or other experiments [59, 131].

IV. ADDITIONAL SHORT-RANGE FOUR-FERMION COUPLING

Besides the long-range Coulomb interaction, there may be various kinds of additional short-range four-fermion couplings [5, 72, 74]. In this section, we study the impact of such short-range couplings on dynamical excitonic gap generation. In principle, there are a number of possible four-fermion couplings, but we shall only consider the following simple one:

$$H_{\rm FF} = \frac{g}{N}\sum_{\sigma=1}^{N}\int d\mathbf{x}\left(\psi_\sigma^\dagger(\mathbf{x})\tau_3\psi_\sigma(\mathbf{x})\right)^2, \tag{22}$$

where g is the quartic coupling constant.

If we ignore the Coulomb interaction and retain the above four-fermion coupling solely, the gap equation takes the form

$$\frac{1}{2g} = \int\frac{d\omega}{(2\pi)}\frac{d^2\mathbf{k}}{(2\pi)^2}\frac{1}{\omega^2+a^2k_x^4+v^2k_y^2+m^2}, \tag{23}$$

where m is supposed to be a constant. Integrating over ω, the gap equation can be further written as

$$\frac{1}{g} = \int\frac{d^2\mathbf{k}}{(2\pi)^2}\frac{1}{\sqrt{a^2k_x^4+v^2k_y^2+m^2}}. \tag{24}$$

By setting $m=0$, we find a critical strength g_c that is determined by the equation

$$\frac{1}{g_c} = \int\frac{d^2\mathbf{k}}{(2\pi)^2}\frac{1}{\sqrt{a^2k_x^4+v^2k_y^2}}. \tag{25}$$

The fermions remain massless if $g<g_c$, but become massive once g exceeds g_c. The critical value g_c is a function of the parameter β, and the dependence of g_c on β is shown in Fig. 7(a). It is clear that g_c is an increasing function of β, with $g_c\to 0$ when $\beta\to 0$. As shown in Fig. 7(b), the fermion mass m increases as g grows from a critical value g_c.

We then incorporate both long-range Coulomb interaction and short-range four-fermion interaction, and obtain the following gap equation:

$$\begin{aligned} m(p_x,p_y) &= \frac{1}{2}\int\frac{d^2\mathbf{k}}{(2\pi)^2}\frac{m(k_x,k_y)}{\sqrt{a^2k_x^4+v^2k_y^2+m^2(k_x,k_y)}} \\ &\quad\times V(\mathbf{p}-\mathbf{k}) \\ &+ g\int\frac{d^2\mathbf{k}}{(2\pi)^2}\frac{m\left(k_x,k_y\right)}{\sqrt{a^2k_x^4+v^2k_y^2+m^2\left(k_x,k_y\right)}}, \end{aligned}$$

where the instantaneous approximation has been adopted to simplify numerical calculations. The dependence gap including both of long-range Coulomb interaction and four-fermion interaction is shown in Fig. 8. We observe that, in the presence of additional four-fermion coupling, the magnitude of excitonic gap is enhanced and the critical value α_c is lowered. If the system contains only four-fermion coupling, there is a critical value $g_c(\beta)$. When both Coulomb and four-fermion interactions are present, α_c takes a finite value smaller than that obtained in the absence of four-fermion coupling, provided that $g<g_c(\beta)$. In the special case of $g>g_c(\beta)$, we find that $\alpha_c=0$, which means an arbitrary weak Coulomb interaction makes an important contribution to excitonic pairing.

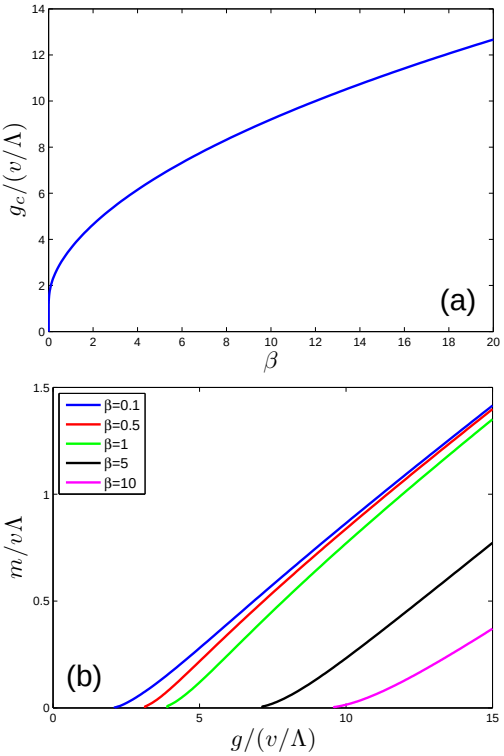

FIG. 7: (a) Dependence of g_c on β. (b) Dependence of m on g at different values of β. Only the four-fermion interaction is considered in this case.

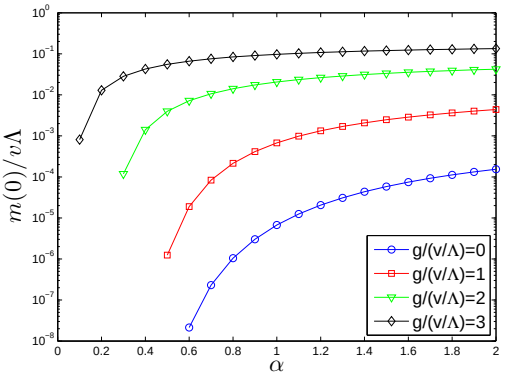

FIG. 8: Dependence of m on α at different values of g. Both the Coulomb and four-fermion interactions are incorporated in the DS equation calculations.

V. QUANTUM CRITICAL PHENOMENA EMERGENT AT INSULATING TRANSITION

Once an excitonic gap is opened at the Fermi level, the semi-Dirac semimetal is converted to an insulator. In order to explicitly see the difference between semimetallic and insulating phases, we shall compute two important quantities, namely fermion DOS and specific heat, in this section. At a given flavor N and fixed β, the insulating quantum phase transition happens at the QCP α_c. A bosonic order parameter ϕ develops a nonzero mean value continuously as α becomes larger than α_c. At such QCP, the semi-Dirac fermions and the excitonic order parameter are gapless, and can strongly affect each other. In this case, one cannot simply integrate out the fermionic degrees of freedom [132, 133]. Instead, one should maintain gapless fermions and gapless bosonic order parameter in an effective action, and study the Yukawa coupling between them [134–139]. In this section, we perform a RG analysis of this coupling, and examine whether the system exhibits NFL behaviors at the QCP.

A. DOS and specific heat in insulating phase

The dynamically generated fermion gap m manifests itself in several observable quantities, among which we are mainly interested in fermion DOS and specific heat. In order to make analytic computation simpler, we assume a constant mass gap m. After including m, the retarded propagator of semi-Dirac fermion is written in the form

$$G^R(\omega,\mathbf{k})=\frac{-1}{\omega-ak_x^2\tau_1-vk_y\tau_2-m\tau_3+i\eta}. \quad (26)$$

The spectral function is given by

$$\begin{aligned} A(\omega,\mathbf{k}) &= \frac{1}{\pi}\mathrm{Tr}\left[\mathrm{Im}\left[G^R(\omega,\mathbf{k})\right]\right] \\ &= 2|\omega|\delta\left(\omega^2-\left(a^2k_x^4+v^2k_y^2+m^2\right)\right). \end{aligned} \quad (27)$$

The fermion DOS can be computed from spectral function:

$$\begin{aligned} \nu(\omega) &= N\int\frac{d^2\mathbf{k}}{(2\pi)^2}A(\omega,\mathbf{k}) \\ &= \frac{K\left(\frac{1}{2}\right)N}{\sqrt{2}\pi^2\sqrt{a}v}\frac{|\omega|}{\left(\omega^2-m^2\right)^{\frac{1}{4}}}\theta\left(|\omega|-m\right), \end{aligned} \quad (28)$$

where $K(x)$ is complete elliptic integrals of the first kind. It is easy to see that DOS is significantly suppressed by the finite gap in the low-energy regime.

To compute specific heat, we find it convenient to work in the Matsubara Green function formalism. The Matsubara propagator of massive semi-Dirac fermions is

$$\begin{aligned} G(\omega_n,\mathbf{k}) &= \frac{1}{-i\omega_n+ak_x^2\tau_1+vk_y\tau_2+m\tau_3} \\ &= \frac{i\omega_n+ak_x^2\tau_1+vk_y\tau_2+m\tau_3}{\left(\omega_n^2+a^2k_x^4+v^2k_y^2+m^2\right)}, \end{aligned} \quad (29)$$

where the imaginary frequency $\omega_n=(2n+1)\pi T$ with n being integers. Accordingly, the free energy of fermions takes the form

$$F(T)=2NT\sum_{\omega_n}\int\frac{d^2k}{(2\pi)^2}\ln\left[\left(\omega_n^2+E_k^2+m^2\right)^{\frac{1}{2}}\right] \quad (30)$$

with $E_k=\sqrt{a^2k_x^4+v^2k_y^2}$. After carrying out the summation over imaginary frequency ω_n, we obtain

$$F(T)=-4NT\int\frac{d^2\mathbf{k}}{(2\pi)^2}\ln\left[1+e^{-\frac{\sqrt{E_k^2+m^2}}{T}}\right], \quad (31)$$

where a temperature independent term has been dropped. The specific heat is connected to the free energy through the relation:

$$C_V(T)=-T\frac{\partial^2}{\partial T^2}F(T). \quad (32)$$

In the gapless semimetallic phase with $m=0$, $C_V(T)$ depends on temperature as

$$C_V(T)=\frac{15\sqrt{2}\left(4-\sqrt{2}\right)K\left(\frac{1}{2}\right)\zeta\left(\frac{5}{2}\right)}{16\pi^{\frac{3}{2}}}\frac{N}{\sqrt{a}v}T^{\frac{3}{2}}, \quad (33)$$

where $\zeta(x)$ is the Riemann zeta function. In the insulating phase with $m\neq 0$, $C_V(T)$ is strongly suppressed by fermion gap comparing to the semimetallic phase. In particular, in the limit $m\gg T$, $C_V(T)$ is given by

$$C_V(T)\approx\frac{4\sqrt{2}K\left(\frac{1}{2}\right)}{3\pi^2}\frac{N}{\sqrt{a}v}\frac{m^{\frac{7}{2}}}{T^2}e^{-\frac{m}{T}}, \quad (34)$$

which decreases rapidly with lowering T.

From Eq. (28) and Eq. (34), we observe that both DOS and specific heat are significantly suppressed in the low-energy region in the insulating phase.

B. Non-Fermi liquid behaviors at semimetal-insulator QCP

In this subsection, we analyze the interaction between the quantum fluctuation of bosonic order parameter ϕ and the gapless semi-Dirac fermions, which is described by a Yukawa-type coupling:

$$S_{fb}=\lambda_0\sum_{\sigma=1}^{N}\int d\tau d^2\mathbf{x}\phi\psi_\sigma^\dagger\tau_3\psi_\sigma. \quad (35)$$

where λ_0 is the coupling coefficient. The free action of ϕ takes the standard form

$$S_\phi=\int d\tau d^2\mathbf{x}\left[\frac{1}{2}\left(\partial_\tau\phi\right)^2+\frac{\kappa}{2}\left(\nabla\phi\right)^2+\frac{r}{2}\phi^2+\frac{u_0}{24}\phi^4\right] \quad (36)$$

where the varying parameter r tunes the excitonic insulating transition with $r = 0$ being QCP. The fee propagator of ϕ is given by

$$D_0(\omega, \mathbf{q}) = \frac{1}{\omega^2 + \kappa \mathbf{q}^2 + r}. \tag{37}$$

Following the treatment of Ref. [138], we now make the replacements: $\phi \to \phi/\lambda_0$ and $r \to r\lambda_0^2$. After doing such a re-scaling manipulation, we write the Yukawa-type coupling as

$$S_{fb} = \sum_{\sigma=1}^{N} \int d\tau d^2\mathbf{x} \phi \psi_\sigma^\dagger \tau_3 \psi_\sigma. \tag{38}$$

It is important to remember that both ϕ and ψ particles are gapless at QCP. The quantum critical behaviors cannot be studied within the Hertz-Millis theory [132, 133]. Alternatively, we need to treat ϕ and ψ on an equal footing and carefully study their coupling [134–139]. We now perform a detailed RG analysis of this coupling by employing a $1/N$ expansion, and examine whether the fermions exhibit NFL behaviors.

At the QCP with $r = 0$, including the polarization function contributed from fermions leads to the following propagator for ϕ field:

$$D(\Omega, \mathbf{q}) = \frac{1}{\omega^2 + \kappa \mathbf{q}^2 + \Pi_{33}(\Omega, \mathbf{q})}, \tag{39}$$

where the polarization Π_{33} is given by

$$\begin{aligned} \Pi_{33}(\Omega, \mathbf{q}) &= N \int \frac{d\omega}{2\pi} \int \frac{d^2\mathbf{k}}{(2\pi)^2} \mathrm{Tr}\left[\tau_3 G_0(\omega, \mathbf{k}) \tau_3 \right. \\ &\left. \times G_0\left(\omega + \Omega, \mathbf{k} + \mathbf{q}\right)\right] \end{aligned} \tag{40}$$

to the leading order of $1/N$ expansion. After straightforward calculations, which are presented in Appendix A, we find that Π_{33} can be approximated by

$$\Pi_{33}(\Omega, \mathbf{q}) = \frac{N}{\sqrt{a}v} \left[b_1 \left(\Omega^2 + v^2 q_y^2\right) + b_2 a^2 q_x^4\right]^{\frac{1}{4}}, \tag{41}$$

where b_1 and b_2 are two constants. In the low-energy regime, Π_{33} dominates over the free term of ϕ. We then drop the free term, and write the propagator as

$$D(\Omega, \mathbf{q}) = \frac{1}{\Pi_{33}(\Omega, \mathbf{q})}. \tag{42}$$

The leading-order fermion self-energy induced by the Yukawa coupling is

$$\begin{aligned} \Sigma_{fb}(\omega, \mathbf{k}) &= \int' \frac{d\Omega}{2\pi} \frac{d^2\mathbf{q}}{(2\pi)^2} \tau_3 G_0\left(\omega + \Omega, \mathbf{k} + \mathbf{q}\right) \\ &\times \tau_3 D(\Omega, \mathbf{q}). \end{aligned} \tag{43}$$

Here, the integration $\int' \frac{d\Omega}{2\pi} \frac{d^2\mathbf{q}}{(2\pi)^2}$ is made by choosing a suitable momentum shell for some related parameter. To be specific, we now employ the following RG scheme:

$$-\infty < \Omega < \infty, \qquad b\Lambda < E_q < \Lambda, \tag{44}$$

where $E_q = \sqrt{a^2 q_x^4 + v^2 q_y^2}$, and $b = e^{-l}$ with l being a running length scale. According to Appendix B, the fermion self-energy takes the approximate form

$$\Sigma_{fb}(\omega, \mathbf{k}) \approx \left[-i\omega C_1 + a k_x^2 C_2 \tau_1 + v k_y C_3 \tau_2\right] \ln(b^{-1}). \tag{45}$$

The expressions of constants $C_{1,2,3}$ are presented in Eqs. (B14)-(B16). Numerical calculation leads us to

$$C_1 \approx -\frac{0.0434929}{N}, \tag{46}$$

$$C_2 \approx -\frac{0.00149482}{N}, \tag{47}$$

$$C_3 \approx -\frac{0.0434929}{N}. \tag{48}$$

Notice that $C_1 = C_3$.

We now proceed to derive the RG equations. The action of free semi-Dirac fermions is

$$\begin{aligned} S_\psi &= \int \frac{d\omega}{2\pi} \frac{dk_x}{(2\pi)} \frac{dk_y}{(2\pi)} \psi^\dagger(\omega, \mathbf{k}) \left(-i\omega + a k_x^2 \tau_1 \right. \\ &\left. + v k_y \tau_2\right) \psi(\omega, \mathbf{k}). \end{aligned} \tag{49}$$

After including the self-energy corrections, this action becomes

$$\begin{aligned} S_\psi &= \int \frac{d\omega}{2\pi} \frac{dk_x}{(2\pi)} \frac{dk_y}{(2\pi)} \psi^\dagger(\omega, \mathbf{k}) \left(-i\omega + a k_x^2 \tau_1 \right. \\ &\left. + v k_y \tau_2 - \Sigma_{fb}(i\omega, \mathbf{k})\right) \psi(\omega, \mathbf{k}) \end{aligned} \tag{50}$$

$$\begin{aligned} &\approx \int \frac{d\omega}{2\pi} \frac{dk_x}{(2\pi)} \frac{dk_y}{(2\pi)} \psi^\dagger(\omega, \mathbf{k}) \left(-i\omega e^{-C_1 l} \right. \\ &\left. + a k_x^2 \tau_1 e^{-C_2 l} + v k_y \tau_2 e^{-C_3 l}\right) \psi(\omega, \mathbf{k}). \end{aligned} \tag{51}$$

We then make the following scaling transformations:

$$k_x = k_x' e^{-\frac{l}{2}}, \tag{52}$$

$$k_y = k_y' e^{-l}, \tag{53}$$

$$\omega = \omega' e^{-l}, \tag{54}$$

$$\psi = \psi' e^{\left(\frac{7}{4} + \frac{C_1}{2}\right) l}, \tag{55}$$

$$a = a' e^{(C_2 - C_1) l}, \tag{56}$$

$$v = v' e^{(C_3 - C_1) l}. \tag{57}$$

Now the action is recast in the form

$$\begin{aligned} S_{\psi'} &= \int \frac{d\omega'}{2\pi} \frac{dk_x'}{(2\pi)} \frac{dk_y'}{(2\pi)} \psi'^\dagger(\omega', \mathbf{k}') \left(-i\omega' + a' k_x'^2 \tau_1 \right. \\ &\left. + v' k_y' \tau_2\right) \psi'(\omega', \mathbf{k}'), \end{aligned} \tag{58}$$

which is formally the same as the action of free fermions. According to Eq. (55), the RG equation for wave function renormalization Z_f satisfies

$$\frac{dZ_f}{dl} = C_1 Z_f. \tag{59}$$

Based on Eqs. (56) and (57), we derive the RG equations for A and v:

$$\frac{da}{dl} = (C_1 - C_2)a, \quad (60)$$
$$\frac{dv}{dl} = (C_1 - C_3)v. \quad (61)$$

Solving the above three RG equations, we obtain

$$Z_f = Z_{f0}e^{C_1 l}, \quad (62)$$
$$a = a_0 e^{(C_1 - C_2)l}, \quad (63)$$
$$v = v_0, \quad (64)$$

where $Z_{f0} = 1$. In the long wavelength limit $l \to \infty$, it is easy to find that Z_f and a both flow to zero, whereas v doest not flow and remains a constant. The behavior $\lim_{l\to\infty} Z_f \to 0$ clearly indicates the breakdown of FL theory. The wave function renormalization Z_f can also be obtained from the identity:

$$Z_f(\omega) = \frac{1}{\left|1 - \frac{\partial}{\partial\omega}\mathrm{Re}\Sigma^R(\omega)\right|}, \quad (65)$$

where $\Sigma^R(\omega)$ is the retarded fermion self-energy function. Combining Eqs. (62) and (65), and then using the scaling relationship $\omega = \omega_0 e^{-l}$, one can find that

$$\mathrm{Re}\Sigma^R(\omega) \sim \omega^{1-\eta_f}, \quad (66)$$

where $\eta_f = -C_1$ is a positive quantity. By virtue of Kramers-Kronig (KK) relation, it is easy to obtain

$$\mathrm{Im}\Sigma^R(\omega) \sim \omega^{1-\eta_f}, \quad (67)$$

which is apparently typical NFL behaviors.

We present a schematic phase diagram in Fig. 9 for 2D interacting semi-Dirac fermion system on the plane spanned by α and T, with α_c defining the semimetal-insulator QCP. The system stays in the gapless semimetal phase for $\alpha < \alpha_c$, and becomes an excitonic insulator for $\alpha > \alpha_c$. The fermions exhibits NFL behaviors at zero-temperature QCP α_c, which becomes a finite quantum critical region at finite temperature.

RG method has recently been applied to study the influence of Coulomb interaction in several semimetals which are distinguished mainly by the fermion dispersions [34, 35, 47–50]. In a 3D anisotropic Weyl semimetal where the spectrum displays quadratic dependence on momentum in one direction but linear dependence on other components of momenta, Yang *et al.* supposed a shell of $(b\Lambda, \Lambda)$ for the integration over the quadratic component of momenta [47]. Lai [48] used the similar RG scheme to examine the impact of Coulomb interaction in a 3D double Weyl semimetal, in which the dispersion is quadratic in two components of momenta but linear in the third component. Different from Lai [48], Jian and Yao [49] considered the same model but made use of a different RG scheme which defines the momentum shell

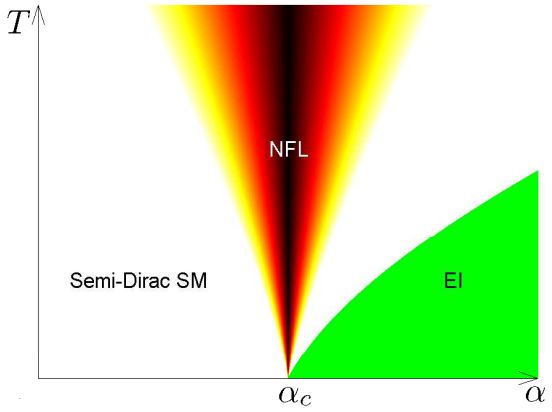

FIG. 9: Schematic phase diagram of semi-Dirac fermion system on plane (α, T) with fixed values of N and β. Here, SM, EI, and NFL stand for semimetal, excitonic insulating, and non-Fermi liquid phases, respectively. The zero-temperature QCP is broadened by thermal fluctuation to a finite quantum critical region on the phase diagram at finite temperatures.

by $b\Lambda < E_q < \Lambda$ with $E_q = \sqrt{\frac{1}{4m^2}(k_x^2 + k_y^2)^2 + v^2 k_z^2}$. The results obtained by Lai [48] and Jian and Yao [49] are not the same. When studying the role of Coulomb interaction in a 2D semi-Dirac semimetal, Isobe *et al.* [34] introduced a shell for energy $b\Lambda < \Omega < \Lambda$, whereas Cho and Moon [35] defined a shell for the linearly dependent momentum component.

Since different RG schemes might give rise to different results, it is useful to carry out RG calculations in several possible manners and then compare the results. In the present problem, we also consider the following three RG schemes:

$$\int'_{\omega,\mathbf{q}} = \int_{-\infty}^{+\infty} d\Omega \left(\int_{-\Lambda}^{-\sqrt{b}\Lambda} + \int_{\sqrt{b}\Lambda}^{\Lambda}\right) dq_x \int_{-\infty}^{+\infty} dq_y, \quad (68)$$
$$\int'_{\omega,\mathbf{q}} = \int_{-\infty}^{+\infty} d\Omega \int_{-\infty}^{+\infty} dq_x \left(\int_{-\Lambda}^{-b\Lambda} + \int_{b\Lambda}^{\Lambda}\right) dq_y, \quad (69)$$
$$\int'_{\omega,\mathbf{q}} = \left(\int_{-\Lambda}^{-b\Lambda} + \int_{b\Lambda}^{\Lambda}\right) d\Omega \int_{-\infty}^{+\infty} dq_x \int_{-\infty}^{+\infty} dq_y, \quad (70)$$

where $\int'_{\omega,\mathbf{q}} \equiv \int' d\omega d^2\mathbf{q}$. For convenience, we hereinafter use RG scheme 1, 2, 3, and 4 to represent Eqs. (44), (68), (69), and (70), respectively. In the RG schemes 2, 3, and 4, the fermion self-energy can still be written as Eq. (45), with the expressions of $C_{1,2,3}$ being given in Appendix C. Numerical calculations show that the values of $C_{1,2,3}$ computed using RG schemes 2, 3, and 4 are precisely the same as those given by Eqs. (46)-(48). Thus, these four different RG schemes all lead to NFL behaviors.

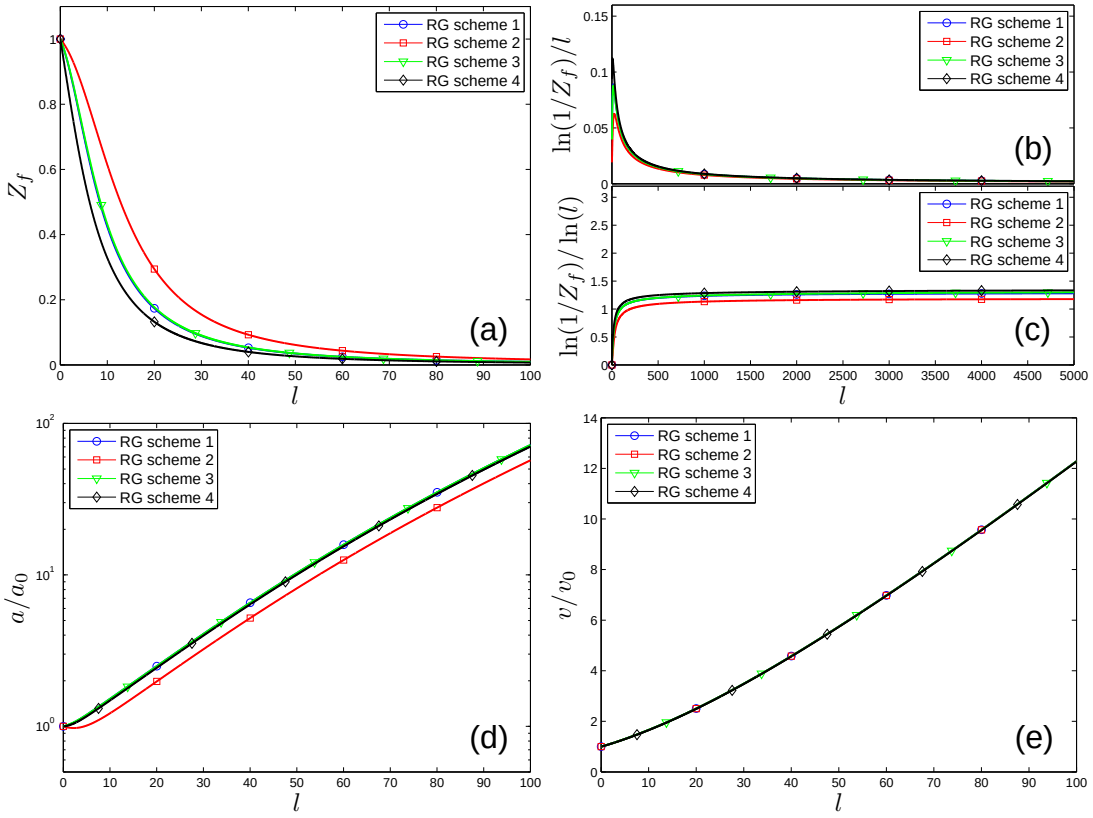

FIG. 10: Flows of Z_f, a, and v considering long-range Coulomb interaction in semimetal phase in different RG schemes. The initial condition $\alpha_0 = 1$ and $\beta_0 = 1$ are taken.

C. Interplay of Yukawa coupling and Coulomb interaction

At semimetal-insulator QCP, semi-Dirac fermions not only couple to the quantum fluctuation of excitonic order parameter ϕ, but interact with each other through the Coulomb interaction. For completeness, it is necessary to consider both the Yukawa coupling and the Coulomb interaction and treat them equally. From the above analysis, we know that Yukawa coupling tends to drive parameter a to decrease upon lowering the energy scale. In contrast, Coulomb interaction can increase a in the low-energy regime. When both Yukawa coupling and Coulomb interaction are present, these two opposite tendencies might give rise to interesting low-energy behaviors of semi-Dirac fermions. This issue will be addressed in this subsection.

In a previous work, Isobe *et al.* studied the influence of Coulomb interaction on semi-Dirac fermions by utilizing the RG scheme Eq. (70). Because different RG schemes may lead to different results [48, 49], we feel it helpful to revisit the effect of Coulomb interaction by employing the four RG schemes defined by Eq. (44), and (68), (69), and (70) respectively. Detailed analytic calculations lead us to

$$\frac{dZ_f}{dl} = C_1' Z_f, \tag{71}$$

$$\frac{da}{dl} = (C_1' - C_2')\, a, \tag{72}$$

$$\frac{dv}{dl} = (C_1' - C_3')\, v, \tag{73}$$

$$\frac{d\alpha}{dl} = (C_3' - C_1')\, \alpha. \tag{74}$$

For RG schemes 1 and 4, β is defined as $\beta = \frac{a\Lambda}{v^2}$, and the RG equation of β can be written as

$$\frac{d\beta}{dl} = (2C_3' - C_1' - C_2' - 1)\, \beta. \tag{75}$$

For RG scheme 2, β is defined as $\beta = \frac{a\Lambda}{v}$, whose RG equation is

$$\frac{d\beta}{dl} = \left(C_3' - C_2' - \frac{1}{2}\right) \beta. \tag{76}$$

For RG scheme 3, β is defined as $\beta = \frac{a\Lambda}{v}$, and the corresponding RG equation is

$$\frac{d\beta}{dl} = (C_3' - C_2' - 1)\, \beta. \tag{77}$$

The expressions of C_1', C_2', and C_3' obtained by employing different RG schemes are given in Appendix D. The RG flows of Z_f, a, v are shown in Fig. 10. According to Fig. 10(a), Z_f obtained by employing four RG schemes

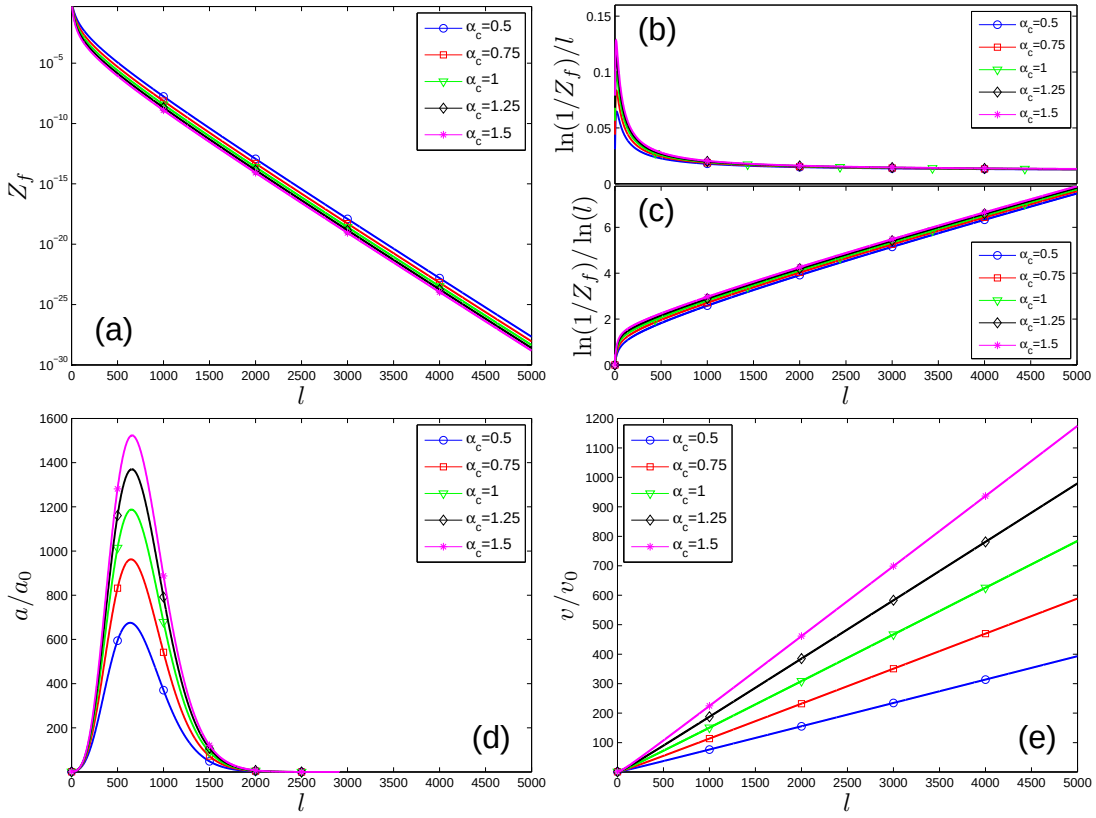

FIG. 11: Flows of Z_f, a, and v considering both of quantum fluctuation of insulating phase and long-range Coulomb interaction at QCP in RG scheme 1. The initial condition $\beta_0 = 1$ is taken.

all flow to zero at large l, thus normal FL description becomes invalid. The l-dependence of Z_f for RG scheme 1 is close to that for RG scheme 3 over a wide range of energies, but different from those obtained by means of RG schemes 2 and 4. Based on Fig. 10(b) and (c), it is easy to verify that

$$\lim_{l\to\infty} \frac{\ln(1/Z_f)}{l} \to 0, \tag{78}$$

but that

$$\lim_{l\to\infty} \frac{\ln(1/Z_f)}{\ln(l)} \to \text{constant}. \tag{79}$$

We see from the above two expressions that Coulomb interaction gives rise to MFL behaviors in the lowest energy limit. This result is qualitatively the same within four different RG schemes, and agrees with the conclusion reached in Ref. [34]. As can be seen from Fig. 10(d) and (e), both a and v increase with growing length scale l. In particular, the numerical results for a are almost identical for RG schemes 1, 3, and 4, but quantitatively larger than the result obtained by RG scheme 2. The numerical results for v in for different RG schemes are all very close to each other.

We then incorporate both the Yukawa coupling and Coulomb interaction, and study their interplay by means of RG method combined with $1/N$ expansion. We will not give the calculational detail here, but only list the final RG equations:

$$\frac{dZ_f}{dl} = (C_1 + C_1')\, Z_f, \tag{80}$$

$$\frac{da}{dl} = (C_1 + C_1' - C_2 - C_2')\, a, \tag{81}$$

$$\frac{dv}{dl} = (C_1' - C_3')\, v, \tag{82}$$

$$\frac{d\alpha}{dl} = (C_3' - C_1')\, \alpha. \tag{83}$$

The RG equation of β are found to be

$$\frac{d\beta}{dl} = (C_3 - C_2 + 2C_3' - C_1' - C_2' - 1)\, \beta \tag{84}$$

for RG schemes 1 and 4,

$$\frac{d\beta}{dl} = \left(C_3 + C_3' - C_2 - C_2' - \frac{1}{2}\right) \beta \tag{85}$$

for RG schemes 2, and

$$\frac{d\beta}{dl} = (C_3 + C_3' - C_2 - C_2' - 1)\, \beta \tag{86}$$

for RG schemes 3.

We present the low-energy behaviors of parameters Z_f, a, and v in Fig. 11 by adopting RG scheme 1 as an example. As shown by Fig. 11(a), Z_f flows monotonously to zero in the lowest energy limit. Using the results displayed in Fig. 11(b) and (c), we find that Z_f manifests the following asymptotic behavior:

$$\lim_{l\to\infty} \frac{\ln(1/Z_f)}{l} \to \text{constant}, \tag{87}$$

and

$$\lim_{l\to\infty} \frac{\ln(1/Z_f)}{\ln(l)} \to \infty. \tag{88}$$

Obviously, the semi-Dirac fermions exhibit NFL behaviors at the semimetal-insulator QCP, so the schematic phase diagram depicted in Fig. 11 is still applicable. We observe from Fig. 11(d) that the parameter a displays a non-monotonic dependence on the length scale l: as l grows, a first increases and then decreases. However, Fig. 11(e) shows that parameter v increases monotonously with growing l. Since v does not flow at all in case there is only Yukawa coupling, the low-energy behavior of v is indeed determined by Coulomb interaction. The numerical results obtained by applying the RG schemes 2, 3, and 4, which are not presented here, are qualitatively the same as those obtained based on RG scheme 1.

VI. SUMMARY AND DISCUSSIONS

In summary, we have studied the possibility of dynamical excitonic gap generation in a 2D semi-Dirac fermion system induced by the long-range Coulomb interaction. The critical interaction strength α_c has been computed by solving the DS equation of dynamical excitonic gap. By employing three frequently used approximations, we have showed that even a moderately strong Coulomb interaction is able to generate a finite excitonic gap. It is therefore much easier for Coulomb interaction to induce excitonic pairing in a 2D semi-Dirac semimetal than a 2D Dirac semimetal. We also have considered the influence of additional short-range interaction, and found that such interaction reduces the value of critical Coulomb interaction strength α_c and therefore catalyzes excitonic gap generation.

Among all the currently known 2D semi-Dirac semimetals, we find that the TiO_2/VO_2 nanostructure is the most promising candidate for the realization of the anticipated excitonic insulating state. There are two reasons. Firstly, 2D semi-Dirac fermions naturally emerge in such a nanostructure, and it is not necessary to elaborately adjust some model parameters. Secondly, the physical value of α in this material is smaller or at least very close to the critical value α_c obtained in our DS equation analysis. It is certainly also possible to open an excitonic gap in other 2D semi-Dirac semimetal materials, which deserves a systematic investigation. We hope that experiments, including but not restricted to ARPES, would be performed in the future to search the predicted excitonic insulating state in various 2D semi-Dirac materials, with TiO_2/VO_2 nanostructure being the most probable candidate.

We also have showed that 2D semi-Dirac fermions exhibit distinct behaviors in the massless semimetal phase, excitonic insulating phase, and at the semimetal-insulator QCP. Specifically, the massless semi-Dirac fermions couple strongly to the quantum fluctuation of excitonic order parameter by a Yukawa-type coupling at the QCP. We have examined the impact of this coupling on the low-energy properties of fermions by carrying out a detailed RG analysis, and revealed unusual NFL behaviors of massless fermions and other interesting quantum critical phenomena.

In the DS equation studies presented in this paper, we have neglected a number of quantities to simplify numerical computation, including the fermion velocity renormalization [75, 79, 80], fermion damping effect [79, 82, 83], and vertex correction [79, 83], which might have non-ignorable effects on the excitonic gap generation. These effects are embodied in the functions $A_{0,1,2}(\omega, k_x, k_y)$ appearing in Eq. (11) and the vertex function $\Gamma(\varepsilon, \mathbf{p}; \omega, \mathbf{k})$ appearing in Eq. (13). Incorporating these quantities in the DS gap equation vastly increases the required time for numerical computations due to the strong anisotropy in the fermion dispersion, and also reduces the precision of the numerical results. This difficulty needs to be solved before reaching a quantitatively more reliable estimate of the critical value α_c. It should be valuable to systematically study the issue of dynamical excitonic gap generation by employing other powerful tools, especially RG approach [43, 87] and large scale Monte Carlo simulation [90–97].

ACKNOWLEDGEMENTS

We would like to acknowledge the financial support by National key Research and Development Program of China under Grant No. 2016YFA0300404, and the support by the National Natural Science Foundation of China under Grants 11504379, 11274286, 11574285, 11674327, and U1532267. J.R.W. is also supported by the Natural Science Foundation of Anhui Province under Grant 1608085MA19.

Appendix A: Calculation of polarization Π_{33}

We now compute the polarization for the coupling between semi-Dirac fermions ψ and quantum fluctuation of insulating order parameter ϕ, which is defined as

$$\Pi_{33}(\Omega,\mathbf{q}) \;=\; N\int\frac{d\omega}{2\pi}\int\frac{d^2\mathbf{k}}{(2\pi)^2}\mathrm{Tr}\left[\tau_3 G_0(\omega,\mathbf{k})\tau_3 G_0\left(\omega+\Omega,\mathbf{k}+\mathbf{q}\right)\right]. \tag{A1}$$

Substituting the fermion propagator Eq. (4) into Eq. (A1), we obtain

$$\Pi_{33}(\Omega,q_x,q_y) \;=\; -2N\int\frac{d\omega}{2\pi}\int\frac{d^2\mathbf{k}}{(2\pi)^2}\frac{\omega\left(\omega+\Omega\right)+a^2k_x^2\left(k_x+q_x\right)^2+v^2k_y\left(k_y+q_y\right)}{\left[\omega^2+a^2k_x^4+v^2k_y^2\right]\left[\left(\omega+\Omega\right)^2+a^2\left(k_x+q_x\right)^4+v\left(k_y+q_y\right)^2\right]}. \tag{A2}$$

Using the Feynman parameterization

$$\frac{1}{AB}=\int_0^1 dx\frac{1}{\left[xA+(1-x)B\right]^2}, \tag{A3}$$

we further write the polarization as

$$\begin{aligned}\Pi_{33}(\Omega,\frac{q_x}{\sqrt{a}},\frac{q_y}{v}) \;=\; & -\frac{2N}{\sqrt{a}v}\int_0^1 dx\int\frac{dk_x}{2\pi}\int\frac{d\omega}{2\pi}\int\frac{dk_y}{2\pi}\\ & \times\left\{\frac{\omega^2+k_y^2-x(1-x)\left(\Omega^2+q_y^2\right)+k_x^2\left(k_x+q_x\right)^2}{\left[\omega^2+k_y^2+x(1-x)\left(\Omega^2+q_y^2\right)+x\left(k_x+q_x\right)^4+(1-x)k_x^4\right]^2}-\frac{1}{\omega^2+k_y^2+k_x^4}\right\},\end{aligned} \tag{A4}$$

where we have made the re-scaling manipulations:

$$q_x\to\frac{q_x}{\sqrt{a}},\;\; k_x\to\frac{k_x}{\sqrt{a}},\;\; q_y\to\frac{q_y}{v},\;\; k_y\to\frac{k_y}{v}. \tag{A5}$$

Moreover, we have used $\Pi_{33}(\Omega,\frac{q_x}{\sqrt{a}},\frac{q_y}{v})-\Pi_{33}(0,0,0)$ to replace $\Pi_{33}(\Omega,\frac{q_x}{\sqrt{a}},\frac{q_y}{v})$ to regularize the polarization function. We then define a new variable $\mathbf{K}=(\omega,k_y)$ and carry out the integration over $\mathbf{K}$, which yields

$$\begin{aligned}&\Pi_{33}(\Omega,\frac{q_x}{\sqrt{a}},\frac{q_y}{v})\\ =\; & -\frac{N}{\pi\sqrt{a}v}\int\frac{dk_x}{2\pi}\left\{\frac{1}{2}\ln\left[\frac{\Lambda^2+\left(k_x+q_x\right)^4}{\left(k_x+q_x\right)^4}\right]+\frac{1}{2}\int_0^1 dx\left[\frac{x\left(\Omega^2+q_y^2\right)+k_x^4-k_x^2\left(k_x+q_x\right)^2}{\Lambda^2+x(1-x)\left(\Omega^2+q_y^2\right)+x\left(k_x+q_x\right)^4+(1-x)k_x^4}\right.\right.\\ & \left.\left.-\frac{x\left(\Omega^2+q_y^2\right)+k_x^4-k_x^2\left(k_x+q_x\right)^2}{x(1-x)\left(\Omega^2+q_y^2\right)+x\left(k_x+q_x\right)^4+(1-x)k_x^4}\right]-\frac{1}{2}\ln\left(\frac{\Lambda^2+k_x^4}{k_x^4}\right)\right\},\end{aligned} \tag{A6}$$

where Λ is an UV cutoff. In the following, we calculate Π_{33} in several different limits.

1. $q_x=0$

In the limit $q_x=0$, we have

$$\Pi_{33}(\Omega,0,\frac{q_y}{v}) \;=\; -\frac{N}{2\pi\sqrt{a}v}\int\frac{dk_x}{2\pi}\int_0^1 dx\left[\frac{x\left(\Omega^2+q_y^2\right)}{\Lambda^2+x(1-x)\left(\Omega^2+q_y^2\right)+k_x^4}-\frac{x\left(\Omega^2+q_y^2\right)}{x(1-x)\left(\Omega^2+q_y^2\right)+k_x^4}\right]. \tag{A7}$$

After integrating over k_x and retaining the leading term, we get

$$\begin{aligned}\Pi_{33}(\Omega,0,\frac{q_y}{v}) \;&=\; \frac{3N\left(\Omega^2+q_y^2\right)^{\frac{1}{4}}}{2\sqrt{2}\pi\sqrt{a}v}\int_0^1 dx\left[x(1-x)\right]^{\frac{1}{4}}\\ &=\; c_1\frac{N}{\sqrt{a}v}\left(\Omega^2+q_y^2\right)^{\frac{1}{4}},\end{aligned} \tag{A8}$$

where $c_1=\frac{\Gamma(\frac{1}{4})}{8\sqrt{\pi}\Gamma(\frac{3}{4})}\approx 0.208657$.

2. $\Omega = 0$ and $q_y = 0$

In the case $\Omega = 0$ and $q_y = 0$, the polarization is given by

$$\begin{aligned}\Pi_{33}(0, \frac{q_x}{\sqrt{a}}, 0) &= -\frac{N}{\pi\sqrt{a}v}\int \frac{dk_x}{2\pi}\left\{\frac{1}{2}\ln\left[\frac{\Lambda^2 + (k_x+q_x)^4}{(k_x+q_x)^4}\right] + \frac{1}{2}\int_0^1 dx\left[\frac{k_x^4 - k_x^2(k_x+q_x)^2}{\Lambda^2 + x(k_x+q_x)^4 + (1-x)k_x^4}\right.\right. \\ &\left.\left. -\frac{k_x^4 - k_x^2(k_x+q_x)^2}{x(k_x+q_x)^4 + (1-x)k_x^4}\right] - \frac{1}{2}\ln\left(\frac{\Lambda^2 + k_x^4}{k_x^4}\right)\right\}, \end{aligned} \tag{A9}$$

Integrating over x and retaining the leading term gives rise to

$$\Pi_{33}(0, \frac{q_x}{\sqrt{a}}, 0) = \frac{N}{4\pi^2\sqrt{a}v}\int_{-\infty}^{+\infty} dk_x \frac{(k_x+q_x)^4 - k_x^2(k_x+q_x)^2}{(k_x+q_x)^4 - k_x^4}\ln\left[\frac{(k_x+q_x)^4}{k_x^4}\right]. \tag{A10}$$

We then assume $k_x = |q_x|\, y$, valid for both positive and negative q_x, and convert Π_{33} to

$$\Pi_{33}(0, \frac{q_x}{\sqrt{a}}, 0) = \frac{N}{4\pi^2}\left\{\int_0^1 dy \frac{y^2}{y^2 + (y-1)^2}\ln\left[\frac{y^4}{(y-1)^4}\right] + \int_0^\infty dy \frac{2y+1}{(y+1)^2 + y^2}\ln\left[\frac{(y+1)^4}{y^4}\right]\right\}\frac{|q_x|}{\sqrt{a}v}, \tag{A11}$$

which leads

$$\Pi_{33}(0, \frac{q_x}{\sqrt{a}}, 0) = c_2 N \frac{|q_x|}{\sqrt{a}v}, \tag{A12}$$

where $c_2 = \frac{1}{4}$.

3. $q_y = 0$ and $\Omega \gg a q_x^2$

In the limit $q_y = 0$, we can expand the polarization in powers of $\frac{aq_x^2}{\Omega}$ and retain the leading and sub-leading terms, which simplifies Π_{33} to the following form

$$\Pi_{33}(\Omega, \frac{q_x}{\sqrt{a}}, 0) = c_1 \frac{N}{\sqrt{a}v}\Omega^{\frac{1}{2}} + \frac{1}{4\pi^2}\frac{N}{\sqrt{a}v}\frac{q_x^2}{\Omega^{\frac{1}{2}}} I_1, \tag{A13}$$

where

$$I_1 = \int_{-\infty}^{+\infty} dy \int_0^1 dx \left[\frac{-y^2}{[x(1-x) + y^4]} + \frac{-6x^2y^2 + 8xy^6}{[x(1-x)+y^4]^2} + \frac{16x^3y^6}{[x(1-x)+y^4]^3}\right] = \frac{5\pi^{\frac{3}{2}}\Gamma(\frac{3}{4})}{8\Gamma(\frac{5}{4})}. \tag{A14}$$

Now Π_{33} can be approximately written as

$$\Pi_{33}(\Omega, \frac{q_x}{\sqrt{a}}, 0) \approx c_1 \frac{N}{\sqrt{a}v}\Omega^{\frac{1}{2}} + c_3 \frac{N}{\sqrt{a}v}\frac{q_x^2}{\Omega^{\frac{1}{2}}} \approx c_1 \frac{1}{\sqrt{a}v}\Omega^{\frac{1}{2}}, \tag{A15}$$

where $c_3 = \frac{5\Gamma(\frac{3}{4})}{32\sqrt{\pi}\Gamma(\frac{5}{4})}$.

4. Ansatz for Π_{33}

According to the polarization calculated in different limits, as shown in Eqs. (A8), (A8), and (A15), we find it appropriate to express Π_{33} by the following ansatz:

$$\Pi_{33}(\Omega, \frac{q_x}{\sqrt{a}}, \frac{q_y}{v}) = \frac{N}{\sqrt{a}v}\left[b_1\left(\Omega^2 + q_y^2\right) + b_2 q_x^4\right]^{\frac{1}{4}}, \tag{A16}$$

where $b_1 = c_1^4$ and $b_2 = c_2^4$. Using the re-scaling relations $\frac{q_x}{\sqrt{a}} \to q_x$ and $\frac{q_y}{v} \to q_y$, we eventually write Π_{33} in the form

$$\Pi_{33}(\Omega, q_x, q_y) = \frac{N}{\sqrt{a}v}\left[b_1\left(\Omega^2 + v^2 q_y^2\right) + b_2 a^2 q_x^4\right]^{\frac{1}{4}}. \tag{A17}$$

Appendix B: Self-Energy of Semi-Dirac fermion

The self-energy of semi-Dirac fermion induced by the quantum fluctuation of excitonic insulating order parameter is defined as

$$\Sigma_{fb}(\omega,\mathbf{k})=\int'\frac{d\Omega}{2\pi}\frac{d^2\mathbf{q}}{(2\pi)^2}\tau_3 G_0\left(\omega+\Omega,\mathbf{k}+\mathbf{q}\right)\tau_3 D(\Omega,\mathbf{q}) \tag{B1}$$

to the leading order of perturbative expansion, where

$$D(\Omega,\mathbf{q})=\frac{1}{\Pi_{33}(\Omega,\mathbf{q})}. \tag{B2}$$

Substituting Eq. (4) into Eq. (B1), we obtain

$$\Sigma_{fb}(\omega,\mathbf{k})=\int'\frac{d\Omega}{2\pi}\frac{d^2\mathbf{q}}{(2\pi)^2}\frac{i\left(\omega+\Omega\right)-a\left(k_x+q_x\right)^2\tau_1-v\left(k_y+q_y\right)\tau_2}{\left(\omega+\Omega\right)^2+a^2\left(k_x+q_x\right)^4+v^2\left(k_y+q_y\right)^2}D(\Omega,\mathbf{q}). \tag{B3}$$

It is easy to verify that

$$\Sigma_{fb}(0,0)=-\int'\frac{d\Omega}{2\pi}\frac{d^2\mathbf{q}}{(2\pi)^2}\frac{aq_x^2\tau_1}{\Omega^2+a^2q_x^4+v^2q_y^2}D(\Omega,\mathbf{q}), \tag{B4}$$

which is not divergent in the lowest energy limit. This constant contribution plays no role in the low-energy region, and thus can be safely dropped in the RG analysis. Expanding $\Sigma_{fb}(\omega,\mathbf{k})$ in powers of small values of $i\omega$, k_x, and k_y, and retaining the leading term, we find that

$$\Sigma_{fb}(\omega,\mathbf{k})\approx(-i\omega)\Sigma_1+ak_x^2\Sigma_2\tau_1+vk_y\Sigma_3\tau_2, \tag{B5}$$

where

$$\Sigma_1 = \int'\frac{d\Omega}{2\pi}\frac{d^2\mathbf{q}}{(2\pi)^2}\frac{\Omega^2-a^2q_x^4-v^2q_y^2}{\left(\Omega^2+a^2q_x^4+v^2q_y^2\right)^2}D(\Omega,\mathbf{q}), \tag{B6}$$

$$\Sigma_2 = \int'\frac{d\Omega}{2\pi}\frac{d^2\mathbf{q}}{(2\pi)^2}\frac{-\Omega^4-3a^4q_x^8+12\Omega^2a^2q_x^4+12a^2q_x^4v^2q_y^2-2\Omega^2v^2q_y^2-v^4q_y^4}{\left(\Omega^2+a^2q_x^4+v^2q_y^2\right)^3}D(\Omega,\mathbf{q}), \tag{B7}$$

$$\Sigma_3 = \int'\frac{d\Omega}{2\pi}\frac{d^2\mathbf{q}}{(2\pi)^2}\frac{-\Omega^2-a^2q_x^4+v^2q_y^2}{\left(\Omega^2+a^2q_x^4+v^2q_y^2\right)^2}D(\Omega,\mathbf{q}). \tag{B8}$$

We now need to perform RG re-scaling manipulations. Firstly, we adopt a RG scheme which integrate over Ω and momenta in the following way:

$$-\infty<\Omega<\infty,\qquad b\Lambda<E_q<\Lambda,\quad\text{with}\quad E_q=\sqrt{a^2q_x^4+v^2q_y^2}, \tag{B9}$$

where $b=e^{-l}$. If we define

$$E_q=\sqrt{a^2q_x^4+v^2q_y^2},\qquad \delta=\frac{aq_x^2}{v\left|q_y\right|}, \tag{B10}$$

the two components of momenta are given by

$$|q_x|=\frac{\sqrt{\delta}\sqrt{E_q}}{\sqrt{a}\left(1+\delta^2\right)^{\frac{1}{4}}},\qquad |q_y|=\frac{E_q}{v\sqrt{1+\delta^2}}. \tag{B11}$$

Therefore, the integration over q_x and q_y can be converted to the integration of over E and δ, through the relation:

$$\begin{aligned} d|q_x|d|q_y| &= \left\|\begin{array}{cc}\frac{\partial|q_x|}{\partial E_q} & \frac{\partial|q_x|}{\partial\delta}\\ \frac{\partial|q_y|}{\partial E_q} & \frac{\partial|q_y|}{\partial\delta}\end{array}\right\| dE_q d\delta \\ &= \left|\frac{\partial|q_x|}{\partial E_q}\frac{\partial|q_y|}{\partial\delta}-\frac{\partial|q_x|}{\partial\delta}\frac{\partial|q_y|}{\partial E_q}\right| dE_q d\delta \\ &= \frac{\sqrt{E_q}}{2v\sqrt{a}\sqrt{\delta}\left(1+\delta^2\right)^{\frac{3}{4}}}dE_q d\delta. \end{aligned} \tag{B12}$$

We now can calculate Eqs. (B6)-(B8) by using the transformations given by Eq. (B11) and Eq. (B12) along with the RG scheme (B9), and obtain

$$\Sigma_1 = C_1 \ln(b^{-1}), \qquad \Sigma_2 = C_2 \ln(b^{-1}), \qquad \Sigma_3 = C_3 \ln(b^{-1}), \tag{B13}$$

where

$$C_1 = \frac{1}{4N\pi^3}\int_{-\infty}^{+\infty} dx \int_0^{+\infty} d\delta \frac{1}{\delta^{\frac{1}{2}}\left(1+\delta^2\right)^{\frac{1}{2}}} \frac{x^2-1}{\left(x^2+1\right)^2}\mathcal{G}(x,\delta), \tag{B14}$$

$$C_2 = \frac{1}{4N\pi^3}\int_{-\infty}^{+\infty} dx \int_0^{+\infty} d\delta \frac{1}{\delta^{\frac{1}{2}}\left(1+\delta^2\right)^{\frac{5}{2}}} \times \frac{-x^4\left(1+\delta^2\right)^2 - 3\delta^4 + 12x^2\delta^2\left(1+\delta^2\right) + 12\delta^2 - 2x^2\left(1+\delta^2\right) - 1}{\left(x^2+1\right)^3}\mathcal{G}(x,\delta), \tag{B15}$$

$$C_3 = \frac{1}{4N\pi^3}\int_{-\infty}^{+\infty} dx \int_0^{+\infty} d\delta \frac{1}{\delta^{\frac{1}{2}}\left(1+\delta^2\right)^{\frac{3}{2}}} \frac{-x^2(1+\delta^2) - \delta^2 + 1}{\left(x^2+1\right)^2}\mathcal{G}(x,\delta), \tag{B16}$$

$$\mathcal{G}^{-1} = \left[b_1 x^2(1+\delta^2) + b_2\delta^2 + b_1\right]^{\frac{1}{4}}. \tag{B17}$$

Appendix C: Calculation of $C_{1,2,3}$ using different RG schemes

As discussed in Sec. V B, there are a number of different RG schemes, which are distinguished by the different manners to integrate over energy and momenta. Here, we provide the expressions for $C_{1,2,3}$ obtained separately by employing these RG schemes.

For the RG scheme

$$\int' d\Omega d^2\mathbf{q} = \int_{-\infty}^{+\infty} d\Omega \left(\int_{-\Lambda}^{-\sqrt{b}\Lambda} + \int_{\sqrt{b}\Lambda}^{\Lambda}\right) dq_x \int_{-\infty}^{+\infty} dq_y, \tag{C1}$$

the expressions of C_i with $(i = 1, 2, 3)$ are given by

$$C_1 = \frac{1}{8N\pi^3}\int_{-\infty}^{+\infty} dx \int_{-\infty}^{+\infty} dy \frac{x^2-1-y^2}{\left(x^2+1+y^2\right)^2}\mathcal{G}(x,y), \tag{C2}$$

$$C_2 = \frac{1}{8N\pi^3}\int_{-\infty}^{+\infty} dx \int_{-\infty}^{+\infty} dy \frac{-x^4-3+12x^2+12y^2-2x^2y^2-y^4}{\left(x^2+1+y^2\right)^3}\mathcal{G}(x,y), \tag{C3}$$

$$C_3 = \frac{1}{8N\pi^3}\int_{-\infty}^{+\infty} dx \int_{-\infty}^{+\infty} \frac{-x^2-1+y^2}{\left(x^2+1+y^2\right)^2}\mathcal{G}(x,y), \tag{C4}$$

$$\mathcal{G}^{-1} = \left[b_1\left(x^2+y^2\right) + b_2\right]^{\frac{1}{4}}. \tag{C5}$$

By virtue of the exchange symmetry between variables x and y, it is easy to find that

$$C_1 = C_3 = \frac{1}{4N\pi^3}\int_{-\infty}^{+\infty} dx \int_{-\infty}^{+\infty} dy \frac{-1}{\left(x^2+1+y^2\right)^2} \frac{1}{\left[b_1\left(x^2+y^2\right)+b_2\right]^{\frac{1}{4}}}. \tag{C6}$$

For the RG scheme given by

$$\int' d\Omega d^2\mathbf{q} = \int_{-\infty}^{+\infty} d\Omega \int_{-\infty}^{+\infty} dq_x \left(\int_{-\Lambda}^{-b\Lambda} + \int_{b\Lambda}^{\Lambda}\right) dq_y, \tag{C7}$$

we accordingly find that

$$C_1 = \frac{1}{4N\pi^3}\int_{-\infty}^{+\infty}dx\int_{-\infty}^{+\infty}dy\frac{x^2-y^4-1}{\left(x^2+y^4+1\right)^2}\mathcal{G}(x,y), \tag{C8}$$

$$C_2 = \frac{1}{4N\pi^3}\int_{-\infty}^{+\infty}dx\int_{-\infty}^{+\infty}dy\frac{-x^4-3y^8+12x^2y^4+12y^4-2x^2-1}{\left(x^2+y^4+1\right)^3}\frac{1}{\left[b_1\left(x^2+1\right)+b_2y^4\right]^{\frac{1}{4}}}\mathcal{G}(x,y), \tag{C9}$$

$$C_3 = \frac{1}{4N\pi^3}\int_{-\infty}^{+\infty}dx\int_{-\infty}^{+\infty}dy\frac{-x^2-y^4+1}{\left(x^2+y^4+1\right)^2}\frac{1}{\left[b_1\left(x^2+1\right)+b_2y^4\right]^{\frac{1}{4}}}\mathcal{G}(x,y), \tag{C10}$$

$$\mathcal{G}^{-1} = \left[b_1\left(x^2+1\right)+b_2y^4\right]^{\frac{1}{4}}. \tag{C11}$$

For the RG scheme

$$\int' d\Omega d^2\mathbf{q} = \left(\int_{-\Lambda}^{-b\Lambda}+\int_{b\Lambda}^{\Lambda}\right)d\Omega\int_{-\infty}^{+\infty}dq_x\int_{-\infty}^{+\infty}dq_y, \tag{C12}$$

we obtain

$$C_1 = \frac{1}{4N\pi^3}\int_{-\infty}^{+\infty}dx\int_{-\infty}^{+\infty}dy\frac{1-x^4-y^2}{\left(1+x^4+y^2\right)^2}\mathcal{G}^{(}x,y), \tag{C13}$$

$$C_2 = \frac{1}{4N\pi^3}\int_{-\infty}^{+\infty}dx\int_{-\infty}^{+\infty}dy\frac{-1-3x^8+12x^4+12x^4y^2-2y^2-y^4}{\left(1+x^4+y^2\right)^3}\mathcal{G}^{(}x,y), \tag{C14}$$

$$C_3 = \frac{1}{4N\pi^3}\int_{-\infty}^{+\infty}dx\int_{-\infty}^{+\infty}dy\frac{-1-x^4+y^2}{\left(1+x^4+y^2\right)^2}\mathcal{G}^{(}x,y), \tag{C15}$$

$$\mathcal{G}^{-1} = \left[b_1\left(1+y^2\right)+b_2x^4\right]^{\frac{1}{4}}. \tag{C16}$$

All the above expressions for $C_{1,2,3}$ are used in Sec. V B to investigate the Yukawa-coupling between the semi-Dirac fermions and the quantum fluctuation of excitonic order parameter at the semimetal-insulator QCP. We find that these different RG schemes lead to essentially the same conclusion.

Appendix D: Expressions of $C'_{1,2,3}$ in four different RG schemes

In RG scheme 1 shown in Eq. (B9), C'_1 can be computed through C_1 shown in Eq. (B14) by replacing $\mathcal{G}(x,\delta)$ with $-\mathcal{G}'(x,\delta)$, and $C'_{2,3}$ can be computed through $C_{2,3}$ shown in Eqs. (B15) and (B16) by replacing $\mathcal{G}(x,\delta)$ with $\mathcal{G}'(x,\delta)$, where $\mathcal{G}'(x,\delta)$ is given by

$$\mathcal{G}'^{-1}(x,\delta) = \frac{\sqrt{\delta+\frac{\beta}{(1+\delta^2)^{\frac{1}{2}}}}}{2\pi N\alpha}+\left[\frac{d_x\delta}{\left(x^2\left(1+\delta^2\right)+c_0\delta^2+1\right)^{\frac{1}{4}}}+\frac{d_y}{\left(x^2\left(1+\delta^2\right)+c_0\delta^2+1\right)^{\frac{3}{4}}}\right], \tag{D1}$$

in which $\beta=\frac{a\Lambda}{v^2}$.

In RG scheme 2 shown in Eq. (C1), C'_1 can be computed through C_1 given by Eq. (C2) by replacing $\mathcal{G}(x,y)$ with $-\mathcal{G}'(x,y)$, and $C'_{2,3}$ can be computed through $C_{2,3}$ given by Eqs. (C3) and (C4) by replacing $\mathcal{G}(x,y)$ with $\mathcal{G}'(x,y)$, where $\mathcal{G}'(x,y)$ can be written as

$$\mathcal{G}'^{-1}(x,y)=\frac{\sqrt{1+\beta^2y^2}}{2\pi N\alpha}+\left[\frac{d_x}{\left(x^2+c_0+y^2\right)^{\frac{1}{4}}}+\frac{d_yy^2}{\left(x^2+c_0+y^2\right)^{\frac{3}{4}}}\right], \tag{D2}$$

in which $\beta=\frac{av}{\Lambda}$.

In RG scheme 3 shown in Eq. (C7), C'_1 can be computed through C_1 given by Eq. (C8) by replacing $\mathcal{G}(x,y)$ with $-\mathcal{G}'(x,y)$, and $C'_{2,3}$ can be computed through $C_{2,3}$ given by Eqs. (C9) and (C10) by replacing $\mathcal{G}(x,y)$ with $\mathcal{G}'(x,y)$, where $\mathcal{G}'(x,y)$ takes the form

$$\mathcal{G}'^{-1}(x,y)=\frac{\sqrt{y^2+\beta}}{2\pi N\alpha}+\left[\frac{d_xy^2}{\left(x^2+c_0y^4+1\right)^{\frac{1}{4}}}+\frac{d_y}{\left(x^2+c_0y^4+1\right)^{\frac{3}{4}}}\right], \tag{D3}$$

in which $\beta = \frac{a\Lambda}{v}$.

In RG scheme 4 shown in Eq. (C12), C_1' can be computed through C_1 shown in Eq. (C13) by replacing $\mathcal{G}(x,y)$ with $-\mathcal{G}'(x,y)$, and $C_{2,3}$ can be computed through $C_{2,3}$ given by Eqs. (C14) and (C15) by replacing $\mathcal{G}(x,y)$ with $\mathcal{G}'(x,y)$, where $\mathcal{G}'(x,y)$ has the expression

$$\mathcal{G}'^{-1}(x,y) = \frac{\sqrt{x^2+\beta y^2}}{2N\pi\alpha} + \left[\frac{d_x x^2}{(1+c_0x^4+y^2)^{\frac{1}{4}}} + \frac{d_y y^2}{(1+c_0x^4+y^2)^{3/4}}\right], \tag{D4}$$

in which $\beta = \frac{a\Lambda}{v^2}$.

[1] O. Vafek and A. Vishwanath, Annu. Rev. Condens. Matter Phys. **5**, 83 (2014).
[2] T. O. Wehling, A. M. Black-Schaffer, and A. V. Balatsky, Adv. Phys. **63**, 1 (2014).
[3] H. Weng, X. Dai, and Z. Fang, J. Phys.:Condens. Matter **28**, 303001 (2016).
[4] A. H. Castro Neto, F. Guinea, N. M. R. Peres, K. S. Novoselov, and A. K. Geim, Rev. Mod. Phys. **81**, 109 (2009).
[5] V. N. Kotov, B. Uchoa, V. M. Pereira, F. Guinea, and A. H. Castro Neto, Rev. Mod. Phys. **84**, 1067 (2012).
[6] M. Z. Hasan and C. L. Kane, Rev. Mod. Phys. **82**, 3045 (2010).
[7] X.-L. Qi and S.-C. Zhang, Rev. Mod. Phys. **83**, 1057 (2011).
[8] S.-Y. Xu, Y. Xia, L. A. Wray, S. Jia, F. Meier, J. H. Dil, J. Osterwalder, B. Slomski, A. Bansil, H. Lin, R. J. Cava, and M. Z. Hasan, Science **332**, 560 (2011).
[9] T. Sato, K. Segawa, K. Kosaka, S. Souma, K. Nakayama, K. Eto, T. Minami, Y. Ando, and T. Takahashi, Nat. Phys. **7**, 840 (2011).
[10] M. Brahlek, N. Bansal, N. Koirala, S.-Y. Xu, M. Neupane, C. Liu, M. Z. Hasan, and S. Oh, Phys. Rev. Lett. **109**, 186403 (2012).
[11] L. Wu, M. Brahlek, R. V. Aguilar, A. V. Stier, C. M. Morris, Y. Lubashevsky, L. S. Bilbro, N. Bansal, S. Oh, and N. P. Armitage, Nat. Phys. **9**, 410 (2013).
[12] Z. K. Liu, B. Zhou, Y. Zhang, Z. J. Wang, H. M. Weng, D. Prabhakaran, S.-K. Mo, Z. X. Shen, Z. Fang, X. Dai, Z. Hussain, and Y. L. Chen, Science **343**, 864 (2014).
[13] M. Neupane, S.-Y. Xu, R. Sankar, N. Alidoust, G. Bian, C. Liu, I. Belopolski, T.-R. Chang, H.-T. Jeng, H. Lin, A. Bansil, F. Chou, and M. Z. Hasan, Nat. Commun. **5**, 3786 (2014).
[14] S. Borisenko, Q. Gibson, D. Evtushinsky, V. Zabolotnyy, B. Büchner, and R. J. Cava, Phys. Rev. Lett. **113**, 027603 (2014).
[15] S. Jeon, B. B. Zhou, A. Gyenis, B. E. Feldman, I. Kimchi, A. C. Potter, Q. D. Gibson, R. J. Cava, A. Vishwanath, and A. Yazdani, Nat. Mater. **13**, 851 (2014).
[16] S.-Y. Xu, I. Belopolski, N. Alidoust, M. Neupane, G. Bian, C. Zhang, R. Sankar, G. Chang, Z. Yuan, C.-C. Lee, S.-M. Huang, H. Zheng, J. Ma, D. S. Sanchez, B. Wang, A. Bansil, F. Chou, P. P. Shibayev, H. Lin, S. Jia, and M. Z. Hasan, Science **349**, 613 (2015).
[17] B. Q. Lv, H. M. Weng, B. B. Fu, X. P. Wang, H. Miao, J. Ma, P. Richard, X. C. Huang, L. X. Zhao, G. F. Chen, Z. Fang, X. Dai, T. Qian, and H. Ding, Phys. Rev. X **5**, 031013 (2015).
[18] B. Q. Lv, N. Xu, H. M. Weng, J. Z. Ma, P. Richard, X. C. Huang, L. X. Zhao, G. F. Chen, C. E. Matt, F. Bisti, V. N. Strocov, J. Mesot, Z. Fang, X. Dai, T. Qian, M. Shi, and H. Ding, Nat. Phys. **11**, 724 (2015).
[19] L. X. Yang, Z. K. Liu, Y. Sun, H. Peng, H. F. Yang, T. Zhang, B. Zhou, Y. Zhang, Y. F. Guo, M. Rahn, D. Prabhakaran, Z. Hussain, S.-K. Mo, C. Felser, B. Yan, and Y. L. Chen, Nat. Phys. **11**, 728 (2015).
[20] S.-Y. Xu, N. Alidoust, I. Belopolski, Z. Yuan, G. Bian, T.-R. Chang, H. Zheng, V. N. Strocov, D. S. Sanchez, G. Chang, C. Zhang, D. Mou, Y. Wu, L. Huang, C.-C. Lee, S.-M. Huang, B. Wang, A. Bansil, H.-T. Jeng, T. Neupert, A. Kaminski, H. Lin, S. Jia, and M. Z. Hasan, Nat. Phys. **11**, 748 (2015).
[21] S.-Y. Xu, I. Beloposki, D. S. Sanchez, C. Zhang, G. Chang, C. Guo, G. Bian, Z. Yuan, H. Lu, T.-R. Chang, P. P. Shibayev, M. L. Prokopovych, N. Alidoust, H. Zheng, C.-C. Lee, S.-M. Huang, R. Sankar, F. Chou, C.-H. Hsu, H.-T. Jeng, A. Bansil, T. Neupert, V. N. Strocov, H. Lin, S. Jian, and M. Z. Hasan, Sci. Adv. **1**, 1501092 (2015).
[22] N. Xu, H. M. Weng, B. Q. Lv, C. E. Matt, J. Park, F. Bisti, V. N. Strocov, D. Gawryluk, E. Pomjakushina, K. Conder, N. C. Plumb, M. Radovic, G. Autès, O. V. Yazyev, Z. Fang, X. Dai, T. Qian, J. Mesot, H. Ding, and M. Shi, Nat. Commun. **7**, 11006 (2016).
[23] D.-F. Xu, Y.-P. Du, Z. Wang, Y.-P. Li, X.-H. Niu, Q. Yao, D. Pavel, Z.-A. Xu, X.-G. Wan, and D.-L. Feng, Chin. Phys. Lett. **32**, 107101 (2015).
[24] S. Souma, Z. Wang, H. Kotaka, T. Sato, K. Nakayama, Y. Tanaka, H. Kimizuka, T. Takahashi, K. Yamauchi, T. Oguchi, K. Segawa, and Y. Ando, Phys. Rev. B **93**, 161112(R) (2016).
[25] S. Nakatsuji, Y. Machida, Y. Maeno, T. Tayama, T. Sakakibara, J. van Duijn, L. Balicas, J. N. Millican, R. T. Macaluso, and J. Y. Chan, Phys. Rev. Lett. **96**, 087204 (2006).
[26] Y. Machida, S. Nakatsuji, S. Onoda, T. Tayama, and T. Sakakibara, Nature **463**, 210 (2010).
[27] B.-J. Yang, M. S. Bahramy, R. Arita, H. Isobe, E.-G. Moon, and N. Nagaosa, Phys. Rev. Lett. **110**, 086402 (2013).
[28] C. Fang, M. J. Gilbert, X. Dai, and B. A. Bernevig, Phys. Rev. Lett. **108**, 266802 (2012).
[29] S.-M. Huang, S.-Y. Xu, I. Belopolski, C.-C. Lee, G.

Chang, T.-R. Chang, B. Wang, N. Alidoust, G. Bian, M. Neupane, D. Sanchez, H. Zheng, H.-T. Jeng, A. Bansil, T. Neupert, H. Lin, and M. Z. Hasan, Proc. Natl. Acad. Sci. U.S.A. **113**, 1180 (2016).
[30] G. Bian, T.-R. Chang, R. Sankar, S.-Y. Xu, H. Zheng, T. Neupert, C.-K. Chiu, S.-M. Huang, G. Chang, I. Belopolski, D. S. Sanchez, M. Neupane, N. Alidoust, C. Liu, B. Wang, C.-C. Lee, H.-T. Jeng, C. Zhang, Z. Yuan, S. Jia, A. Bansil, F. Chou, H. Lin, and M. Z. Hasan, Nat. Commun. **7**, 10556 (2016).
[31] Y. Wu, L.-L. Wang, E. Mun, D. D. Johnson, D. Mou, L. Huang, Y. Lee, S. L. Bud'ko, P. C. Canfield, and A. Kaminski, Nat. Phys. **12**, 667 (2016).
[32] L. M. Schoop, M. N. Ali, C. Straßer, A. Topp, A. Varykhalov, D. Marchenko, V. Duppel, S. S. P. Parkin, B. V. Lotsch, and C. R. Ast, Nat. Commun. **71**, 11696 (2016).
[33] J. Hu, Z. Tang, J. Liu, X. Liu, Y. Zhu, D. Graf, K. Myhro, S. Tran, C. N. Lau, J. Wei, and Z. Mao, Phys. Rev. Lett. **117**, 016602 (2016).
[34] H. Isobe, B.-J. Yang, A. Chubukov, J. Schmalian, and N. Nagaosa, Phys. Rev. Lett. **116**, 076803 (2016).
[35] G. Y. Cho and E.-G. Moon, Sci. Rep. **6**, 19198 (2016).
[36] A. Sekine, T. Z. Nakano, Y. Araki, and K. Nomura, Phys. Rev. B **87**, 165142 (2013).
[37] M. Sitte, A. Rosch, and L. Fritz, Phys. Rev. B **88**, 205107 (2013).
[38] P. Goswami and S. Chakravarty, Phys. Rev. Lett. **107**, 196803 (2011).
[39] P. Hosur, S. A. Parameswaran, and A. Vishwanath, Phys. Rev. Lett. **108**, 046602 (2012).
[40] R. E. Throckmorton, J. Hofmann, E. Barnes, and S. Das Sarma, Phys. Rev. B **92**, 115101 (2015).
[41] J. González, Phys. Rev. B **90**, 121107(R) (2014).
[42] E.-G. Moon, C. Xu, Y. B. Kim, and L. Balents, Phys. Rev. Lett. **111**, 206401 (2013).
[43] I. F. Herbut and L. Janssen, Phys. Rev. Lett. **113**, 106401 (2014).
[44] L. Janssen and I. F. Herbut, Phys. Rev. B **92**, 045117 (2015).
[45] P. T. Dumitrescu, Phys. Rev. B **92**, 121102 (R) (2015).
[46] L. Janssen and I. F. Herbut, Phys. Rev. B **93**, 165109 (2016).
[47] B.-J. Yang, E.-G. Moon, H. Isobe, and N. Nagaosa, Nat. Phys. **10**, 774 (2014).
[48] H.-H. Lai, Phys. Rev. B **91**, 235131 (2015).
[49] S.-K. Jian and H. Yao, Phys. Rev. B **92**, 045121 (2015).
[50] Y. Huh, E.-G. Moon, and Y. B. Kim, Phys. Rev. B **93**, 035138 (2016).
[51] H. Isobe and N. Nagaosa, Phys. Rev. Lett. **116**, 116803 (2016).
[52] R. Shankar, Rev. Mod. Phys. **66**, 129 (1994).
[53] J. González, F. Guinea, and M. A. H. Vozmediano, Nucl. Phys. B **424**, 595 (1994).
[54] J. González, F. Guinea, and M. A. H. Vozmediano, Phys. Rev. B **59**, 2474(R) (1999).
[55] D. T. Son, Phys. Rev. B **75**, 235423 (2007).
[56] J. Hofmann, E. Barnes, and S. Das Sarma, Phys. Rev. Lett. **113**, 105502 (2014).
[57] C. Bauer, A. Rückriegel, A. Sharma, and P. Kopietz, Phys. Rev. B **92**, 121409(R) (2015).
[58] A. Sharma and P. Kopietz, Phys. Rev. B **93**, 235425 (2016).
[59] D. C. Elias, R. V. Gorbachev, A. S. Mayorov, S. V. Morozov, A. A. Zhukov, P. Blake, L. A. Ponomarenko, I. V. Grigorieva, K. S. Novoselov, F. Guinea, and A. K. Geim, Nat. Phys. **7**, 701 (2011).
[60] D. A. Siegel, C.-H. Park, C. Hwang, J. Deslippe, A. V. Fedorov, S. G. Louie, and A. Lanzara, Proc. Natl. Acad. Sci. U.S.A. **108**, 11365 (2011).
[61] G. L. Yu, R. Jalil, B. Belle, A. S. Mayorov, P. Blake, F. Schedin, S. V. Morozov, L. A. Ponomarenko, F. Chiappini, S. Wiedmann, U. Zeitler, M. I. Katsnelson, A. K. Geim, K. S. Novoselov, and D. C. Elias, Proc. Natl. Acad. Sci. U.S.A. **110**, 3282 (2013).
[62] L. Miao, Z. F. Wang, W. Ming, M.-Y. Yao, M. Wang, F. Yang, Y. R. Song, F. Zhu, A. V. Fedorov, Z. Sun, C. L. Gao, C. Liu, Q.-X. Xue, C.-X. Liu, F. Liu, D. Qian, and J.-F. Jia, Proc. Natl. Acad, Sci. U.S.A. **110**, 2758 (2013).
[63] T. Kondo, M. Nakayama, R. Chen, J. J. Ishikawa, E.-G. Moon, T. Yamamoto, Y. Ota, W. Malaeb, H. Kanai, Y. Nakashima, Y. Ishida, R. Yoshida, H. Yamamoto, M. Matsunami, S. Kimura, N. Inami, K. Ono, H. Kumigashira, S. Nakatsuji, L. Baltents, and S. Shin, Nat. Commun. **6**, 10042 (2015).
[64] D. V. Khveshchenko, Phys. Rev. Lett. **87**, 246802 (2001).
[65] A. H. Castro Neto, Physics **2**, 30 (2009).
[66] V. A. Miransky, *Dynamical Symmetry Breaking in Quantum Field Theories*, (World Scientific, 1993).
[67] Y. Nambu and G. Jona-Lasinio, Phys. Rev. **122**, 345 (1961).
[68] C.-X. Zhang, G.-Z. Liu, and M.-Q. Huang, Phys. Rev. B **83**, 115438 (2011).
[69] C.-X. Zhang, G.-Z. Liu, and X.-G. Qiu, unpublished (2016).
[70] E. V. Gorbar, V. P. Gusynin, V. A. Miransky, and I. A. Shovkovy, Phys. Rev. B **66**, 045108 (2002).
[71] D. V. Khveshchenko and H. Leal, Nucl. Phys. B **687**, 323 (2004).
[72] G.-Z. Liu, W. Li, and G. Cheng, Phys. Rev. B **79**, 205429 (2009).
[73] D. V. Khveshchenko, J. Phys.:Condens. Matter **21**, 075303 (2009).
[74] O. V. Gamayun, E. V. Gorbar, and V. P. Gusynin, Phys. Rev. B **81**, 075429 (2010).
[75] J. Sabio, F. Sols, and F. Guinea, Phys. Rev. B **82**, 121413(R) (2010).
[76] G.-Z. Liu and J.-R. Wang, New J. Phys. **13**, 033022 (2011).
[77] J.-R. Wang and G.-Z. Liu, J. Phys. Condens. Matter **23**, 155602 (2011).
[78] J.-R. Wang and G.-Z. Liu, J. Phys. Condens. Matter **23**, 345601 (2011).
[79] J.-R. Wang and G.-Z. Liu, New J. Phys. **14**, 043036 (2012).
[80] C. Popovici, C. S. Fischer, and L. von Smekal, Phys. Rev. B **88**, 205429 (2013).
[81] J.-R. Wang and G.-Z. Liu, Phys. Rev. B **89**, 195404 (2014).
[82] J. González, Phys. Rev. B **92**, 125115 (2015).
[83] M. E. Carrington, C. S. Fischer, L. von Smekal, and M. H. Thoma, Phys. Rev. B **94**, 125102 (2016).
[84] O. V. Gamayun, E. V. Gorbar, and V. P. Gusynin, Phys. Rev. B **80**, 165429 (2009).
[85] J. Wang, H. A. Fertig, G. Murthy, and L. Brey, Phys. Rev. B **83**, 035404 (2011).

[86] A. Katanin, Phys. Rev. B **93**, 035132 (2016).
[87] O. Vafek and M. J. Case, Phys. Rev. B **77**, 033410 (2008).
[88] J. González, Phys. Rev. B **82**, 155404 (2010).
[89] J. González, Phys. Rev. B **85**, 085420 (2012).
[90] J. E. Drut and T. A. Lähde, Phys. Rev. Lett. **102**, 026802 (2009).
[91] J. E. Drut and T. A. Lähde, Phys. Rev. B **79**, 165425 (2009).
[92] J. E. Drut and T. AL. Lähde, Phys. Rev. B **79**, 241405(R) (2009).
[93] W. Armour, S. Hands, and C. Strouthos, Phys. Rev. B **81**, 125105 (2010).
[94] W. Armour, S. Hands, and C. Strouthos, Phys. Rev. B **84**, 075123 (2011).
[95] P. V. Buividovich and M. I. Polikarpov, Phys. Rev. B **86**, 245117 (2012).
[96] M. V. Ulybyshev, P. V. Buividovich, M. I. Katsnelson, and M. I. Polikarpov, Phys. Rev. Lett. **111**, 056801 (2013).
[97] D. Smith and L. von Smekal, Phys. Rev. B **89**, 195429 (2014).
[98] A. S. Mayorov, D. C. Elias, I. S. Mukhin, S. V. Morozov, L. A. Ponomarenko, K. S. Novoselov, A. K. Geim, and R. V. Gorbachev, Nano. Lett. **12**, 4629 (2012).
[99] T. O. Wehling, E. Sasioğlu, C. Friedrich, A. I. Lichtenstein, M. I. Katsnelson, and S. Blügel, Phys. Rev. Lett. **106**, 236805 (2011).
[100] Y. Hasegawa, R. Konno, H. Nakano, and M. Kohmoto, Phys. Rev. B **74**, 033413 (2006).
[101] P. Dietl, F. Piéchon, and G. Montambaux, Phys. Rev. Lett. **100**, 236405 (2008).
[102] M. O. Goerbig, J.-N. Fuchs, G. Montambaux, and F. Piéchon, Phys. Rev. B **78**, 045415 (2008).
[103] G. Montambaux, F. Piéchon, J.-N. Fuchs, and M. O. Goerbig, Eur. Phys. J. B **72**, 509 (2009).
[104] G. Montambaux, F. Piéchon, J.-N. Fuchs, and M. O. Goerbig, Phys. Rev. B **80**, 153412 (2009).
[105] A. Kobayashi, S. Katayama, Y. Suzumura, and H. Fukuyama, J. Phys. Soc. Jpn. **76**, 034711 (2007).
[106] A. Kobayashi, Y. Suzumura, F. Piéchon, and G. Montambaux, Phys. Rev. B **84**, 075450 (2011).
[107] K. Dolui and S. Y. Quek, Sci. Rep. **5**, 11699 (2015).
[108] S. Yuan, E. van Veen, M. I. Katsnelson, and R. Roldán, Phys. Rev. B **93**, 245433 (2016).
[109] S. S. Baik, K. S. Kim, Y. Yi, and H. J. Choi, Nano. Lett. **15**, 7788 (2015).
[110] B. Wunsch, F. Guinea, and F. Sols, New. J. Phys. **10**, 103027 (2008).
[111] L.-K. Lim, J.-N. Fuchs, and G. Montambaux, Phys. Rev. Lett. **108**, 175303 (2012).
[112] L. Tarruell, D. Greif, T. Uehlinger, G. Jotzu, and T. Esslinger, Nature **483**, 302 (2012).
[113] M. Bellec, U. Kuhl, G. Montambaux, and F. Mortessagne, Phys. Rev. Lett. **110**, 033902 (2013).
[114] J. Kim, S. S. Baik, S. H. Ryu, Y. Sohn, S. Park, B.-G. Park, J. Denlinger, Y. Yi, H. J. Choi, and K. S. Kim, Science **349**, 723 (2015).
[115] V. Pardo and W. E. Pickett, Phys. Rev. Lett. **102**, 166803 (2009).
[116] V. Pardo and W. E. Pickett, Phys. Rev. B **81**, 035111 (2010).
[117] S. Banerjee, R. R. P. Singh, V. Pardo, and W. E. Pickett, Phys. Rev. Lett. **103**, 016402 (2009).
[118] C. Kamal and M. Ezawa, Phys. Rev. B **91**, 085423 (2015).
[119] C. Wang, Q. Xia, Y. Nie, M. Rahman, and G. Guo, AIP Adv. **6**, 035204 (2016).
[120] B. Dóra, I. F. Herbut, and R. Moessner, Phys. Rev. B **88**, 075126 (2013).
[121] C. D. Roberts and A. G. Williams, Prog. Part. Nucl. Phys. **33**, 477 (1994).
[122] C. D. Roberts and S. M. Schmidt, Prog. Part. Nucl. Phys. **42**, **S1** (2000).
[123] T. Appelquist, D. Nash, and L. C. R. Wijewardhana, Phys. Rev. Lett. **60**, 2575 (1988).
[124] T. Appelquist and L. C. R. Wijewardhana, arXiv:hep-ph/0403250.
[125] G.-Z. Liu and G. Cheng, Phys. Rev. D **67**, 065010 (2003).
[126] C. S. Fischer, R. Alkofer, T. Dahm, and P. Maris, Phys. Rev. D **70**, 073007.
[127] H.-T. Feng, F.-Y. Hou, X. He, W.-M. Sun, and H.-S. Zong, Phys. Rev. D **73**, 016004 (2006).
[128] J.-R. Wang, G.-Z. Liu, and C.-J. Zhang, Phys. Rev. D **91**, 045006 (2015) and the references there in.
[129] Z. Yang, C. Ko, V. Balakrishnan, G. Gopalakrishnan, and S. Ramanathan, Phys. Rev. B **82**, 205101 (2010).
[130] M. Hashimoto, I. M. Vishik, R.-H. He, T. P. Devereaux, and Z.-X. Shen, Nat. Phys. **10**, 483 (2014).
[131] L. Taillefer, Annu, Rev. Condens. Matter Phys. **1**, 51 (2010).
[132] J. A. Hertz, Phys. Rev. B **14**, 1165 (1976).
[133] A. J. Millis, Phys. Rev. B **48**, 7183 (1993).
[134] M. A. Metlitski and S. Sachdev, Phys. Rev. B **82**, 075127 (2010); M. A. Metlitski and S. Sachdev, Phys. Rev. B **82**, 075128 (2010);
[135] M. Garst and A. V. Chubukov, Phys. Rev. B **81**, 235105 (2010).
[136] L. Savary, E.-G. Moon, and L. Balents, Phys. Rev. X **4**, 041027 (2014).
[137] S.-K. Jian, Y.-F. Jiang, and H. Yao, Phys. Rev. Lett. **114**, 237001 (2015).
[138] Y. Huh and S. Sachdev, Phys. Rev. B **78**, 064512 (2008).
[139] J. Wang, G.-Z. Liu, and H. Kleinert, Phys. Rev. B **83**, 214503 (2011).